1-1-1990

A laser diode magnetostrictive Terfenol-D magnetometer

Russell Wing-Chiu Chung
Iowa State University

A Laser Diode Magnetostrictive Terfenol-D Magnetometer

by

Russell Wing-Chiu Chung

A Thesis Submitted To the
Graduate Faculty in Partial Fulfillment of the
Requirements for the Degree of
MASTER of SCIENCE

Department: Electrical Engineering and Computer Engineering
Major: Electrical Engineering

Approve

Signatures have been redacted for privacy

For the Graduate College

Iowa State University
Ames, Iowa

1990

TABLE OF CONTENTS

LIST OF FIGURES

ABSTRACT

A sensitive and miniature magnetic field intensity measuring device is desired since people have become concerned about the effect of magnetic fields on health. Such a device cannot be constructed with a conventional fiber optic sensor which is too complex and bulky to be used as a portable device. In this research work, a magnetostrictive magnetometer was fabricated with a piece of Terfenol-D rod and a low-cost laser diode. The prototype has demonstrated very promising results, indicating that such a device is capable of meeting the requirements of simplicity of design and high sensitivity. The use of Terfenol-D as a transducer in a magnetic field intensity measurement is reported for the first time. Also, an experimental study on the diode sensor provided information that cannot be found in the literature. Laser diode sensor modelling is discussed in order to explore further the principles of the magnetometer.

1. INTRODUCTION

1.1 Overview

Recently, people have become concerned about the biological effects of magnetic fields on human beings and, therefore, there is a need for a portable magnetic field measuring device. Various instruments are available for serving such purposes. However, all of the available devices measure the magnetic field strength by an induced EMF technique. The sensitivity of this technique depends on the cross-sectional area of the induction coil as well as the the total number of turns in the coil. It may be difficult to achieve a sensitive device and a reasonable size with the induced EMF technique. Recently, optical detection techniques implemented with single mode optical fibers and diode lasers have demonstrated micro-Oersted range sensitivity which can hardly be achieved by electronic techniques. However, fiber optic sensors cannot meet the requirements of simplicity of design, ruggedness of construction, and miniaturization or portability of the entire measuring system. Therefore, highly sensitive fiber optic sensors have not been produced commercially and are used in laboratory environment only. A miniature, yet relatively sensitive device using an optical detection scheme is desired for research work in field measurement of the magnetic field intensity.

1.2 Problem Statement

The goal of this research work was to seek a 'proof of concept' of a portable, yet relatively sensitive magnetic field measuring device based on the optical detection scheme.

1.3 General Overview

In Chapter 2, the necessary physics to understand the principles of a laser and its modelling are discussed. Although this research work is related to semiconductor diode lasers, the operating principles of the diode laser are briefly discussed in Chapter 3. It was found that a proper understanding of conventional laser physics was much more important and helpful in reading current literature than understanding semiconductor laser physics. Chapter 4 discusses the basic elements of the magnetometer, which includes a magnetic field transducer, a sensor and the necessary electronics. The detail of the implementation of the magnetometer prototype and the preliminary evaluation results are covered in Chapter 5. Furthermore, Chapter 5 reports an experimental study on the laser diode sensor and contains experimental results that are reported for the first time. Chapter 6 discusses the modelling aspect of the diode laser sensor.

2. REVIEW OF LASER PHYSICS

2.1 Atomic Radiation

2.1.1 Einstein's A and B coefficient

A. Einstein identified three radiative processes that are responsible for the generation of electromagnetic energy in an atomic system [1]. These processes are spontaneous emission, absorption and stimulated emission. The above processes lay the fundamentals of laser operation and are discussed in detail in the following context relating to a two-level system as shown in Fig. 2.1.

(a) Spontaneous emission

As the name implies, spontaneous emission describes the process by which the electrons in level 2 (see Fig. 2.1) decayed spontaneously to level 1. In doing so, these electrons emit energy in the form of a photon. If the density of population in level 2 is N_2, the decay of this level can be modelled as

$$dN_2/dt \text{ spontaneous emission} = -A_{21}N_2 \qquad (2.1.1)$$

This equation implies that if no other process took place, the atomic population would decrease with a time constant $t=1/A_{21}$. Also, the population at level 1 increases as fast as level 2 decreases because electrons leaving level 2 can only go to level 1 in this model, and hence $dN_1/dt = -dN_2/dt$.

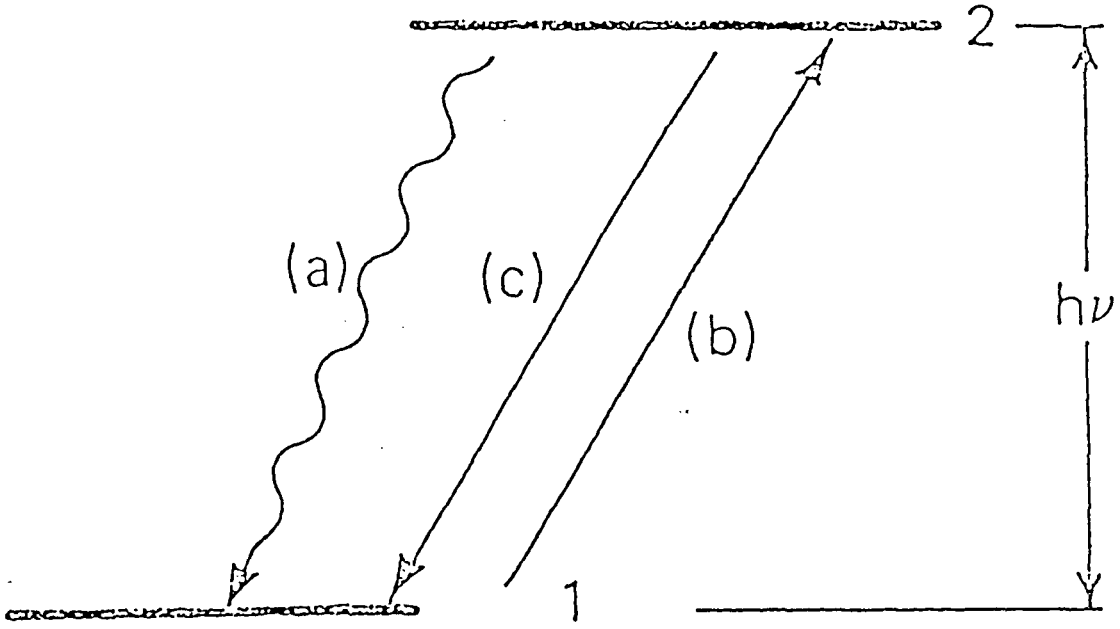

Fig. 2.1 A two-level atomic system (a) spontaneous emission (b) absorption (c) stimulated emission

(b) Absorption

In this process, electrons in level 1 absorb a photon and converts itself into one of the electrons in level 2. The rate at which this process takes place depends on the number of absorbing electrons and the field from which they extract energy. The rate equation for this process can be written as

$$\left(\frac{dN_2}{dt}\right)_{\text{absorption}} = +B_{21}N_1\rho(\nu) = -\left(\frac{dN_1}{dt}\right)_{\text{absorption}} \qquad (2.\ 1.\ 2)$$

where N_2 is the population density at level 2, N_1 is the population density at level 1, $\rho(\nu)$ is the energy density of the field, B_{21} is a constant.

(c) Stimulated emission

This process is the reverse of absorption. The electron gives up its energy to the field, adding coherently to the intensity. Thus the added photon is at the same frequency, at the same phase, in the same sense of polarization, and propagates in the same direction as the wave that induced the electron transition. The rate equation for this process depends on the number of electrons to be stimulated and the strength of the stimulating field.

$$\left(\frac{dN_2}{dt}\right)_{\substack{\text{stimulated}\\ \text{emission}}} = -B_{21}N_2\rho(\nu) = -\left(\frac{dN_1}{dt}\right)_{\substack{\text{stimulated}\\ \text{emission}}} \qquad (2.\ 1.\ 3)$$

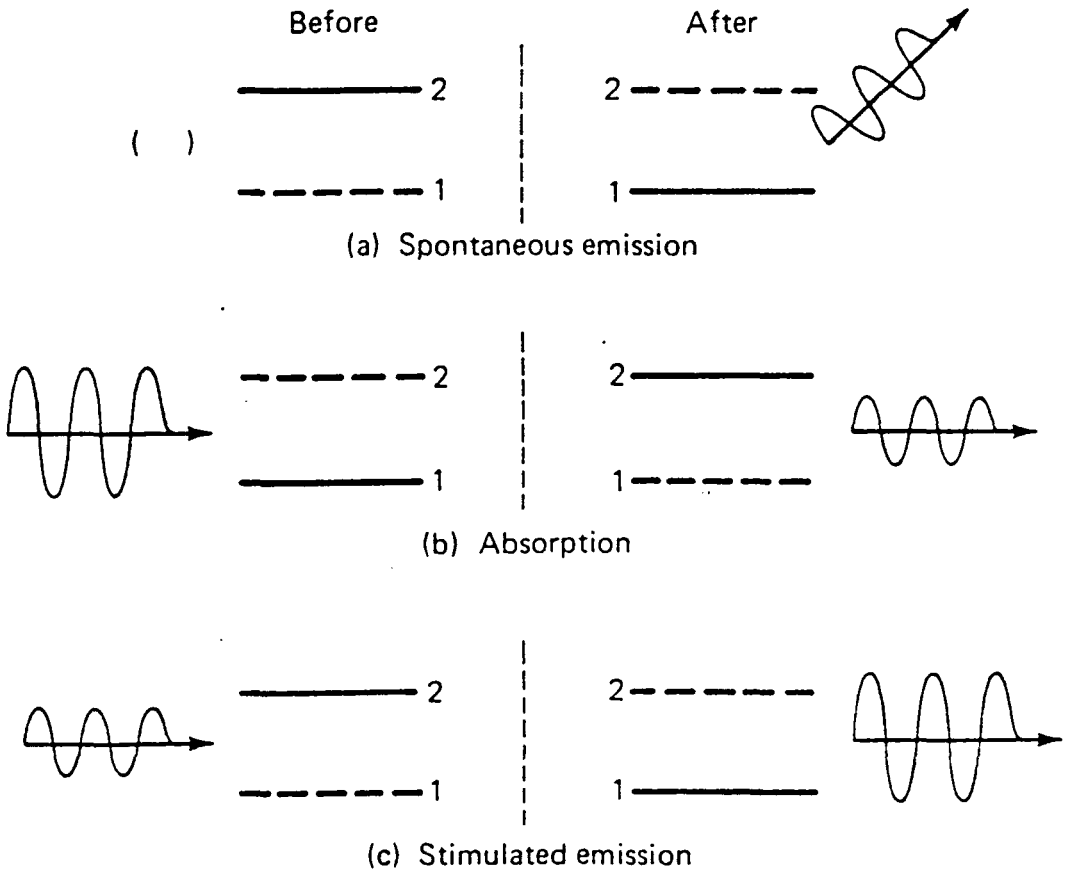

Fig. 2.2 Radiative processes in a two levels electronic system: (a) Spontaneous emission (b) Absorption (c) Stimulated emission

These three processes are shown in Figs. 2.2a, 2.2b and Fig. 2.2c. The spontaneous emission in Fig. 2.2a can radiate into any of 4π steradians with any sense of polarization. In the absorption process, part of the incoming wave is not absorbed and continues along the path. The picture for absorption is just the reverse of the stimulated emission.

2.1.2 Relationship between the A and B coefficients

By defining the above radiative processes, Einstein was able to reproduce the black body radiation formula. At thermodynamic equilibrium, the rate of going 'down' must be balanced by the rate of going 'up'. That is,

$$\frac{dN_2}{dt} = \frac{dN_1}{dt} \tag{2. 1. 4}$$

and

$$\frac{dN_2}{dt} = -A_{21}N_2 + B_{21}N_1\rho(\nu) - B_{21}N_2\rho(\nu) \tag{2. 1. 5}$$

At equilibrium, the time rate of change must be zero. Therefore,

$$\frac{N_2}{N_1} = \frac{B_{12}\rho(\nu)}{A_{21} + B_{21}\rho(\nu)} \tag{2. 1. 6}$$

Equation (2. 1. 6) represents the population density ratio of level 1 to level 2. One can also invoke classical Boltzman statistics to provide another equation on the ratio:

$$\frac{N_2}{N_1} = e^{-\frac{h\nu}{kT}}$$

(2. 1. 7)

where k= Boltzman constant,T=temperature in Kelvin, h=Planck's constant, ν is the frequency of radiation.

Comparing equation (2. 1. 7) and (2. 1. 6), the energy density function, $\rho(\nu)$, can be expressed as:

$$\rho(\nu) = \frac{A_{21}}{B_{21}} \times \frac{1}{\frac{B_{12}}{B_{21}} e^{\frac{h\nu}{kT}} - 1}$$

(2. 1. 8)

To reproduce the black body radiation formula derived by Max Planck in Eisberg [2],

$$\rho(\nu) = \frac{8\pi n^3 \nu^2}{c^3} \cdot \frac{h\nu}{e^{\frac{h\nu}{kT}} - 1}$$

(2. 1. 9)

Einstein concluded that the ratio of B_{12} to B_{21} was one, and consequently

$$\frac{A_{21}}{B_{21}} = \frac{8\pi I^3 h \nu^3}{c^3}$$

(2. 1. 10)

where I=0,1,2.....

The above equation is very useful because it relates spontaneous emission to stimulated emission. Furthermore, the above equation is derived under the assumption that B_{12}/B_{21} is equal to one, therefore the absorption coefficient is also known. In other words, if one of the coefficients (i.e., A_{21}, B_{12} or B_{21}) is known, all are known.

2.1.3 Line shape function

In the previous analysis, the derivation started by using the idea of discrete energy states in an electron. But if these energy states were perfectly sharp, the uncertainty principle would indicate an infinite indeterminacy in the time that the electron is in one of these states. Therefore, the energy-level picture is forced to be modified. This is accomplished by smearing the energy levels into a sharply peaked band, as shown in **Fig. 2.3**. Although the diagram greatly exaggerates the broadening of the energy levels, it emphasizes that radiation does appear on either side of the line center. **Fig. 2.3** also emphasizes the fact that different energy levels have different broadening. The bell-shaped curves representing the energy levels can be interpreted as the relative probability of an electron being found in a band dE_2 around energy E_2, given that the electron is at level 2. Since transitions can occur between dE_2 and dE_1, the radiation spectrum is also broadened.

Mathematically, a line shape function, g(ν) is needed to account for the spectral broadening. The line shape function is defined such that g(ν)dν is the probability of emission of a photon with frequency between ν and ν + dν. If the atoms emits a photon, it has to appear somewhere. So the integrated probability must be unity,

$$\int_0^{\infty} g(\nu)d\nu = 1 \qquad (2.1.11)$$

Although the limit of integration is from zero to infinity, one can expect the main contribution to be in a very narrow band about ν_{21}. A detail discussion on a line shape function is given in reference **[3]**. Generally speaking, one can classify the broadening process into two categories: homogeneous broadening and inhomogenous broadening. If every atom were more or less the same as any other one, or there were no distinguishing feature about any one group, the broadening mechanism is known as homogeneous broadening. On the other hand, if there is a characteristic that distinguishes one group of atoms from another, the broadening mechanism is called inhomogenous broadening. In the case of inhomogenous broadening, different groups of atoms are distinguished by different frequency responses. One example of inhomogenous broadening is the Doppler broadening, in which different groups of atoms have different velocity components.

The idea of a line shape is very important and is summarized here:

The line-shape function ,g(ν)dν , is the relative probability that:

a. A photon emitted by a spontaneous transition will appear between ν and ν + dν.

b. Radiation in the frequency interval ν to ν + dν can be absorbed by atoms in state 1.

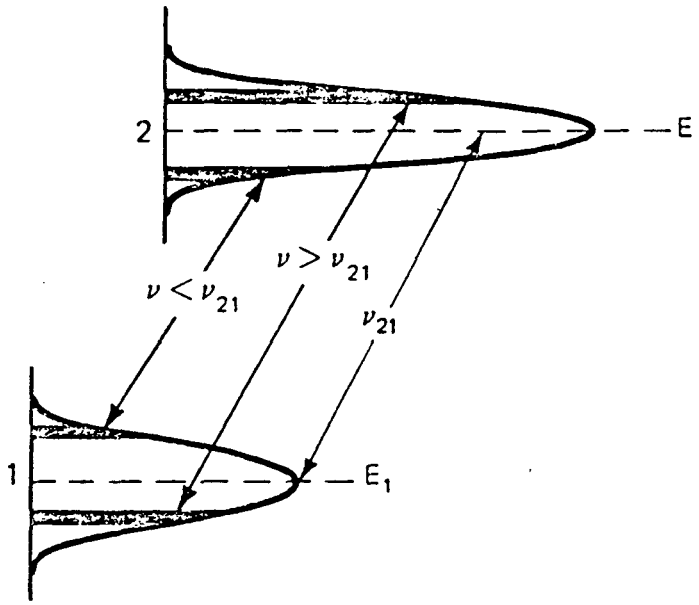

Fig. 2.3 Modification of energy level

c. Radiation in this interval will stimulate atoms in level 2 to give up their internal energy.

The above three conditions involve spontaneous emission (i.e., condition a), absorption (i.e., condition b), and stimulated emission (i.e., condition c). However, the same line-shape function applies to all these processes. It should be noted that in reality the line-shape function may have a complicated form, and may even be mathematically intractable.

This subsection has briefly summarized the background material useful in the operation of a laser using a two level atomic system as an example. The concepts of Einstein's A and B coefficients are introduced, the principal radiative mechanisms (i.e., spontaneous emission, stimulated emission and absorption) are discussed, and the concept of line shape function is examined.

2.2 Laser Oscillation and Amplification

2.2.1 A modified description of transition rates

In the previous section, the Einstein coefficients were introduced, and in the derivation, there exists an energy density function, $\rho(\nu)$, which accounts for the interaction of a continuous radiation spectrum with the discrete energy levels of a group of atoms. The inclusion of an energy density function implies that the bandwidth of the radiation (i.e., energy spread) is much larger than the band of emission or absorption. However, in dealing with lasers, one usually has a finite amount of radiant energy per unit volume in a bandwidth that is much smaller than the corresponding spread expressed by the line shape of the transition. Therefore, the application of the energy density function in the derivation needs to

be modified. For example, the rate of change of the population at level 2 as a result of a monochromatic wave at a frequency ν with energy density ρ_ν is now written as:

$$\left(\frac{dN_2}{dt}\right)_{\substack{\text{absorption} \\ \text{stimulated emission}}} = -N_2 B_{21} g(\nu)\,\rho_\nu + N_1 B_{12} g(\nu)\,\rho_\nu \qquad (2.2.1)$$

Rather than using energy density, ρ_ν, it is useful to talk in terms of intensity (i.e., Watts/unit area). The intensity can be obtained from energy density by recognizing that electromagnetic energy travels at the velocity c/n, where c is the speed of light and n is the refractive index of the material. Therefore,

$$I_n = \frac{c}{n}\rho_\nu \qquad (2.2.2)$$

and equation (2.2.1) can be re-written as:

$$\left(\frac{dN_2}{dt}\right)_{\substack{\text{stimulate emission} \\ \text{absorption}}} = -A_{21}\frac{\lambda_0^2}{8\pi n^2} g(\nu) \cdot (N_2 - N_1)\frac{I_\nu}{h\nu} \qquad (2.2.3)$$

It should be noted that $I_\nu/h\nu$ is just the number of photons passing a unit area per unit time, and is better known as photon flux.

2.2.2 Amplification by an atomic system

Consider a beam of monochromatic light passing through an optical medium, and suppose the medium contains electrons in energy level 1 and energy level 2. In the previous analysis on the A and B coefficients, one can easily see that the rate of stimulated emission will exceed the absorption rate if the population at level 2 is bigger than the population at level 1. That is,

$$N_2 > N_1 \tag{2. 2. 4}$$

Such a condition is contrary to the thermal equilibrium distribution given by Boltzman's equation, and this condition is known as population inversion. Usually, an external pumping agent is required to achieve or maintain the population inversion condition. The pumping process may be in the form of electrical pumping, optical pumping or some other means [4]. If one can maintain the population inversion in an optical medium while a beam of monochromatic radiation (with a proper frequency) passes through it, the medium will amplify the incoming radiation.

One can imagine an experiment in which a slab of inverted material, Δz long, is being irradiated by an incoming polarized electromagnetic wave with intensity I_ν, and the outgoing radiation is detected by a photodetector. The experiment setup is shown in Fig. 2.4. One must note that the photodetector in this experiment cannot distinguish between the various physical processes involved. For example, a photon radiated spontaneously by the slab, and reaching the photodetector gives the same response as a photon produced by stimulated emission. Therefore, spontaneous emission from this slab contributes noise in the

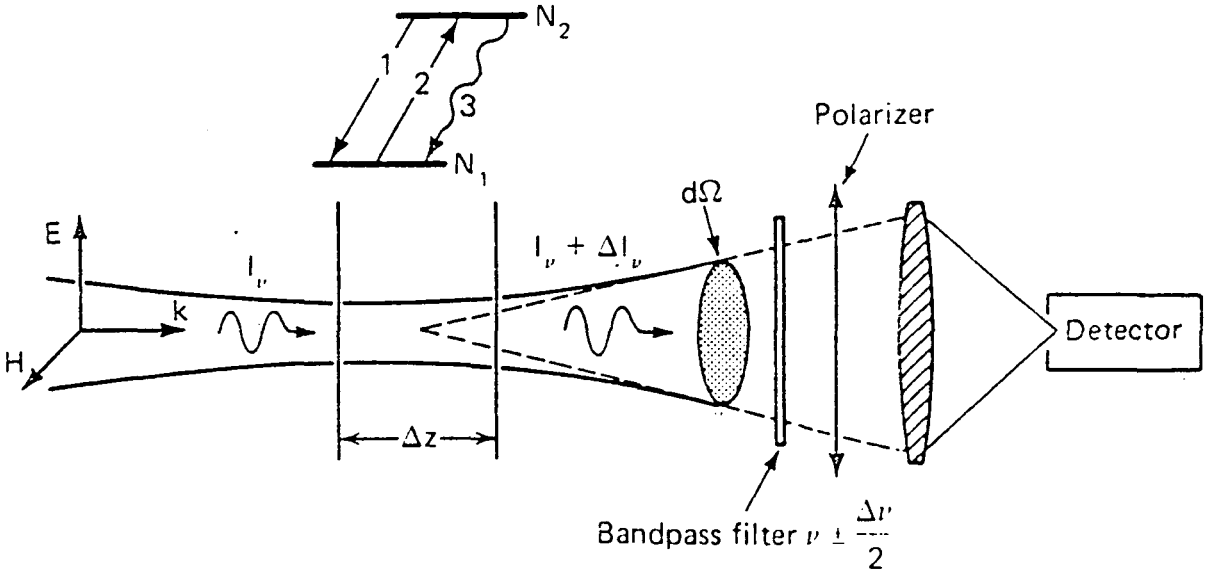

Fig. 2.4 A generic optical amplifier

experiment. To enhance the signal-to-noise ratio of this experiment, one can limit the bandwidth of the photodetector by some sort of a filter with a passband delta ν around the frequency ν of the source. Also, one can put in a polarizer to reject one half of the spontaneous emission power, and one can limit the field of view to match the incoming beam. With these modifications, the output now consists of the input intensity plus stimulated emission plus spontaneous emission minus absorption. One can formulate the change in intensity as:

$$\begin{aligned}\Delta I_\nu &= h\nu \cdot B_{21}\frac{I_\nu}{c}\cdot g(\nu)\cdot N_2\Delta z \\ &- h\nu \cdot B_{12}\frac{I_\nu}{c}\cdot g(\nu)\cdot N_1\Delta z \\ &+ h\nu \cdot A_{21}\Delta\nu \cdot g(\nu)\cdot \frac{1}{2}\cdot \frac{d\Omega}{4\pi}\cdot N_2\Delta z\end{aligned} \qquad (2.\ 2.\ 5)$$

Further manipulating of equation (2. 2. 5), gives the following expression to model the change in intensity per Δz as:

$$\begin{aligned}\frac{\Delta I_\nu}{\Delta z} &= \left[\frac{h\nu}{c}(B_{21}N_2 - B_{12}N_1)g(\nu)\right]I_\nu \\ &+ \frac{1}{2}\left[h\nu A_{21}N_2 g(\nu)\Delta\nu\frac{d\Omega}{4\pi}\right]\end{aligned} \qquad (2.\ 2.\ 6)$$

The second term on the right hand side is the noise term from spontaneous emission since this signal is present even if there is no input signal. This noise term is essential to initiate the

oscillation in the laser. It is convenient to use a gain coefficient and rewrite equation (2. 2. 6) as follow:

$$\frac{dI_\nu}{dz} = \left[A_{21}\frac{\lambda_0^2}{8\pi n^2} g(\nu)(N_2 - N_1)\right] I_\nu \triangleq \text{gain}(\nu) I_\nu$$

(2. 2. 7)

It should be noted that the above gain coefficient is the 'small-signal' coefficient. In other words, the incoming intensity is sufficiently small that the populations of level 2 and level 1 are negligibly perturbed. One can integrate equation (2. 2. 7) to obtain

$$\begin{aligned} I_\nu &= I_\nu(0)\exp[\text{gain}(\nu)z] \\ &= G_o(\nu) I_\nu(0) \\ G_o &= \exp[\text{gain}(\nu)d] \end{aligned}$$

(2. 2. 8)

The gain coefficient G_0 is interpreted as the small signal power gain of an amplifier of length d. One important point of the gain coefficient is its frequency dependent property. Strictly speaking, different gain coefficients needs to be assigned to each incoming intensity with different frequencies.

2.2.3 Threshold for laser oscillation

In the previous section, an inverted system is discussed and the system behaves as an narrow band amplifier. To make an amplifier into an oscillator, one must provide a proper feedback to the amplifier. A simple way of doing this is shown in Fig. 2.5. The condition for which an amplifier with feedback behaves as an oscillator is known as the threshold condition. The threshold for oscillation exists when the round-trip gain of the amplifier is greater or equal to one. To complete one round trip, the light intensity is amplified twice, and part of the power is lost as the light reflects from each mirror. Mathematically, this can be represented as:

$$R_1 R_2 e^{2 \cdot \text{gain}(\nu) \cdot d} \geq 1 \qquad (2.2.9)$$

where R_1 and R_2 are the reflectivities at mirror 1 and mirror 2 and d is the length of the amplifier medium. One can rearrange equation (2. 2. 9) to obtain the threshold figure for the gain coefficient as:

$$\text{gain}_\nu \geq \frac{1}{2d} \ln\left(\frac{1}{R_1 R_2}\right) = \text{Loss} \qquad (2.2.10)$$

where Loss is the loss per unit length.

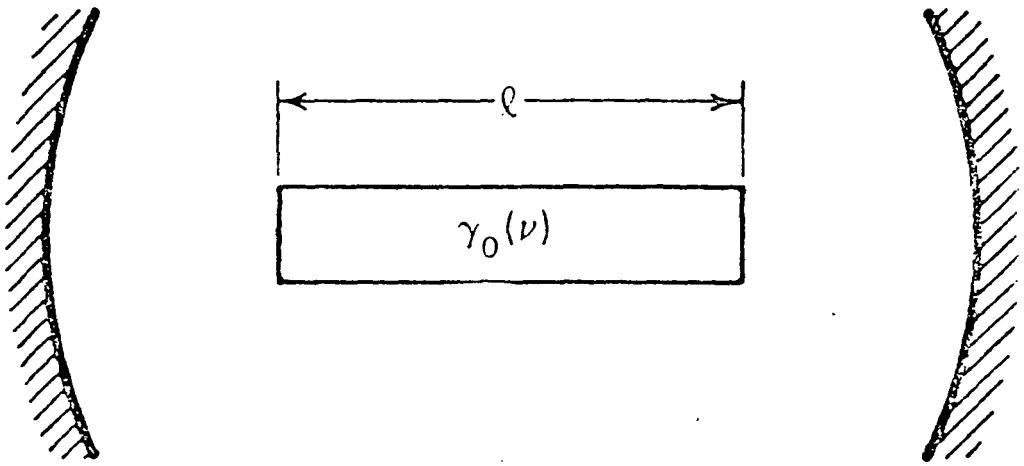

Fig. 2.5 A simple laser system with amplifier and feedback mirror

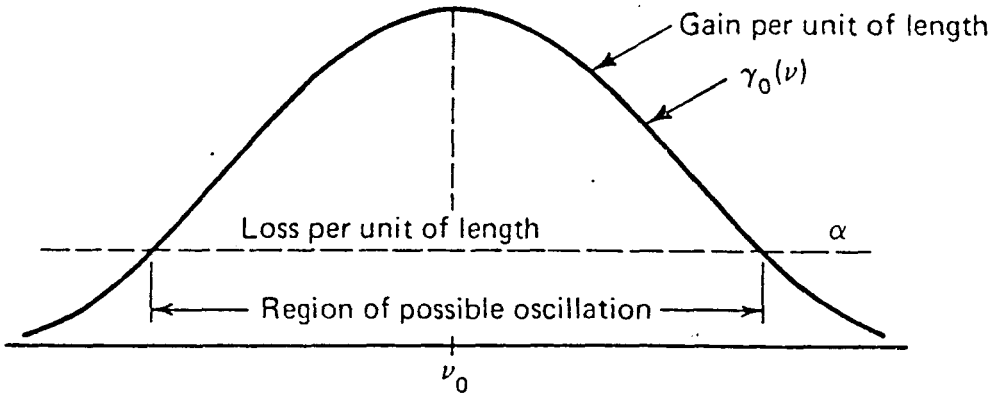

Fig. 2.6 Graphical solution of the threshold inequality

Equation (2. 2. 10) implies that there is a considerable range of frequencies for which the inequality is satisfied. (A graphical solution for equation (2. 2. 10) is shown in **Fig. 2.6.**) This fact is transparent if one remembers that the gain coefficient is a function of the line shape function, and therefore laser oscillation can take place in a relatively wide range of frequency. However, laser oscillation will occur at a discrete frequency decided by the cavity mode that has the highest gain-to-loss ratio. In the case of the plane mirror reflector, the cavity is similar to a Fabry-Perot interferometer. The pass bands of the Fabry-Perot resonator occur at some equally spaced frequencies. These frequencies differ by the free spectral range given by:

$$\text{Free Spectral Range} = \frac{c}{2 \cdot d \cdot n_g} \qquad (2.\ 2.\ 11)$$

where c is the speed of light, n_g is the group refractive index, and d is the length of the cavity. The longitudinal modes of the cavity are given by integer multiples of equation (2. 2. 11).

2.2.4 Laser oscillation in a homogenous broadened material

As mentioned in the previous section, once the threshold condition is met, laser oscillation can take place. However, the homogenous broadened gain curve implies that oscillation can take place in a range of frequencies. Nevertheless, laser oscillation is observed to take place at discrete frequencies. This section explains the physics involved in the oscillation process.

At the start-up of oscillation, the medium is inverted and spontaneous emission has already filled the cavity with radiation at all sorts of frequencies. However, due to the Fabry-

Perot resonator, not all frequencies can exist in the cavity, only those which coincide with the longitudinal mode of the Fabry-Perot cavity modes. Nevertheless, there is a very good chance that the spontaneous emission produces photons which match the cavity mode. Consequently, a standing wave pattern is formed. At the beginning of oscillation, the fields in the cavity modes are just beginning to form as a result of spontaneous emission. These resonant fields are amplified by stimulated emission. Those close to the line center and which match the gain profile are amplified after travelling back and forth in the cavity. The fields which lie in the cavity modes but not so close to the center of the line shape function get amplified to a lesser extent. After a number of round trips, the intensity at the line center frequency will have been amplified to a significant amount but the intensity cannot grow indefinitely. The amplification process implies that the population density at level 2 is being depleted, and the population inversion must have decreased. When the stimulated field grows to a certain extent, it causes the electrons at level 2 to give up their energy as fast as they are being pumped up to level 2. A steady state condition is reached eventually. Therefore, the gain of the system must change to a lower value until the rate of production of the excess inverted population is balanced by the rate of stimulated emission. This phenomenon is known as gain saturation. The above physical process is of utmost important in laser oscillation, and is summarized as follow:

a. The laser gain coefficient saturates at a value slightly lower than the loss, with the difference being made up by the spontaneous emission, at the frequency of oscillation. The shape of the gain function is similar to the initial one but the peak value is reduced (because this is a homogeneously broadened system).

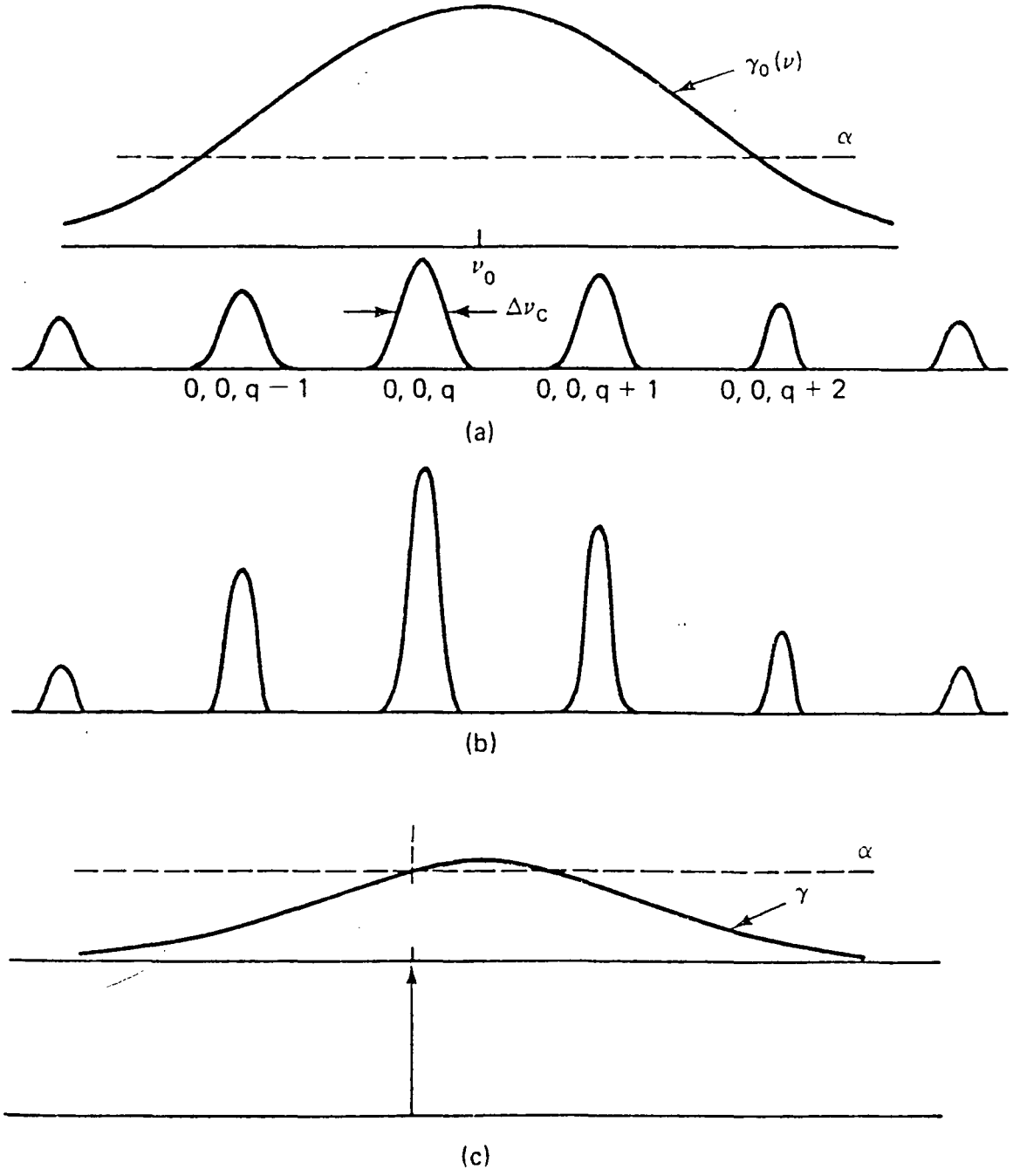

Fig. 2.7 Evolution of laser oscillation from spontaneous emission (a) initial (b) intermediate (c) final

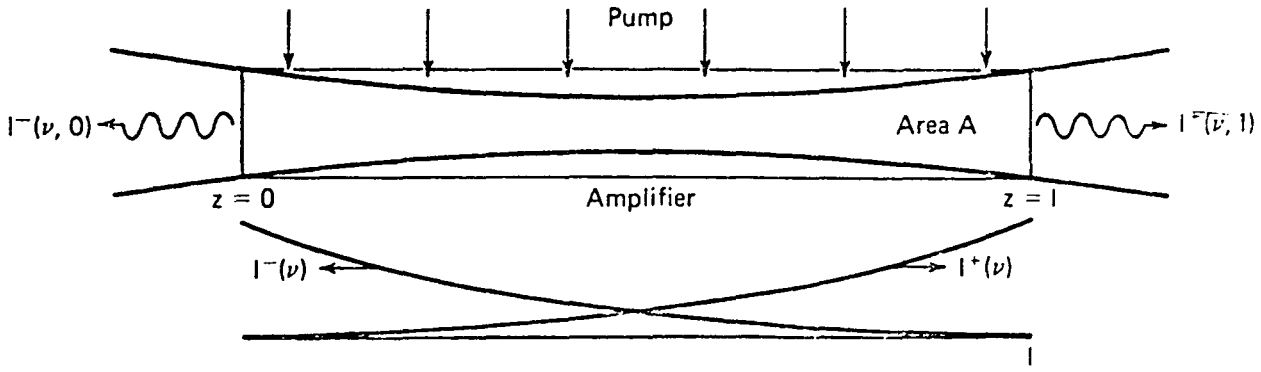

Fig. 2.8 Optical amplifier with ASE

b. The spectral power of emission has changed, with the central mode much larger than the others. Those modes that suffer a loss rather than gain due to the saturation phenomena are supported by the spontaneous emission only.

c. Laser oscillation occurs at the center of the cavity mode which has the highest net gain.

The evolution of laser oscillation from spontaneous emission is shown in Fig. 2.7. It should be noted that laser oscillation in an inhomogeneous system is quite different since spectral hole burning is involved.

2.2.5 Amplified spontaneous emission (ASE)

Consider an inverted medium as shown in Fig. 2.8. The atoms at level 2 may radiate spontaneously into a frequency interval coinciding with the cavity mode and which matches the gain profile of the inverted medium. Light intensity, resulting from the spontaneous emission, can travel in a positive or negative direction. At z=0, an atom may radiate spontaneously, and part of its energy is amplified by the inversion between z=0 and z=l. Thus, part of the spontaneous emission energy is being amplified. Also, spontaneous emission continually adds to this amplified intensity along z. This energy contributed by spontaneous emission is undesirable in an optical amplifier since the ASE drains some of the inverted atoms and helps saturating the gain. In a laser oscillator, the ASE effect should be included into the modelling of laser operation [5].

3. SEMICONDUCTOR DIODE LASER

The previous chapter is devoted to the physics of laser operation and most of the concepts are related to an inverted electron system. Although this research work deals with a semiconductor diode laser, most of the knowledge of the inverted electron system applies to the laser diode. In addition, a sound background in conventional laser physics is essential in understanding much of the semiconductor laser literature. The purpose of this chapter is to provide a general review of a semiconductor diode laser.

3.1 General Review

The semiconductor laser diode is one of the most important types of laser systems being used today. Semiconductor laser diodes use a semiconductor as the lasing medium and are capable of direct modulation up into the gigahertz range. In addition, diode lasers are relatively low cost and compact. The basic mechanism for light emission from a semiconductor material has been studied extensively [6]. A laser diode utilizes the recombination of electrons and holes at a pn junction to produce coherent emission as a dc current passes through the diode. Similar to other electronic laser systems, three radiative processes are involved. Instead of using electronic levels 1 and 2 as in the previous discussion, one talks about bands in a semiconductor (i.e., conductor bands and valence bands). The three important radiative processes are:

a. Absorption: an electron in the valence band can absorb the incident radiation and be excited to the conduction band leading to the generation of an electron-hole pair.

b. Spontaneous emission: an electron can make make a spontaneous transition in which it recombines with a hole.

c. Stimulated emission: incident radiation stimulates an electron in the conduction band to make a transition to the valence band and emit coherent light.

As discussed in the previous chapter, to achieve a laser oscillator, one needs an inverted medium and a proper feedback mechanism. To produce an inverted medium, one needs a pumping agent. In a semiconductor laser diode, the pumping mechanism is the forward bias of the pn junction. Under forward bias, a large density of electrons is created in the bottom of the conduction band and simultaneously, in the same region of space, a large density of holes is created at the top of the valence band (see **Fig. 3.1**). When an optical beam with a frequency slightly greater than E_g/h, where E_g is the bandgap energy, passes through the medium, the beam will be amplified through a stimulated emission process. To make the amplifying medium into a laser, one must provide a feedback mechanism, which is usually done by cleaving or polishing the ends of the pn junction diode at right angles to the junction. The threshold value for oscillation is reached as the gain overcomes the losses in the diode cavity. Therefore, one will expect a threshold current magnitude in the laser diode.

The early laser diode was based on a pn junction formed in the same semiconductor material by proper doping and these are referred to as homojunction lasers. However, these laser diodes required a very large threshold current and could operate only at liquid helium temperature. A significant reduction in threshold current densities was achieved by heterojunction technology. A heterojunction is a junction formed between two dissimilar semiconductors. Today, most of the laser diodes are based on a double heterojunction structure in which a thin layer of a semiconductor with a narrow bandgap is sandwiched between two larger bandgap semiconductors. This is shown in **Fig. 3.2a**. One special feature of the double heterostructure is the optical confinement in the active layer because the

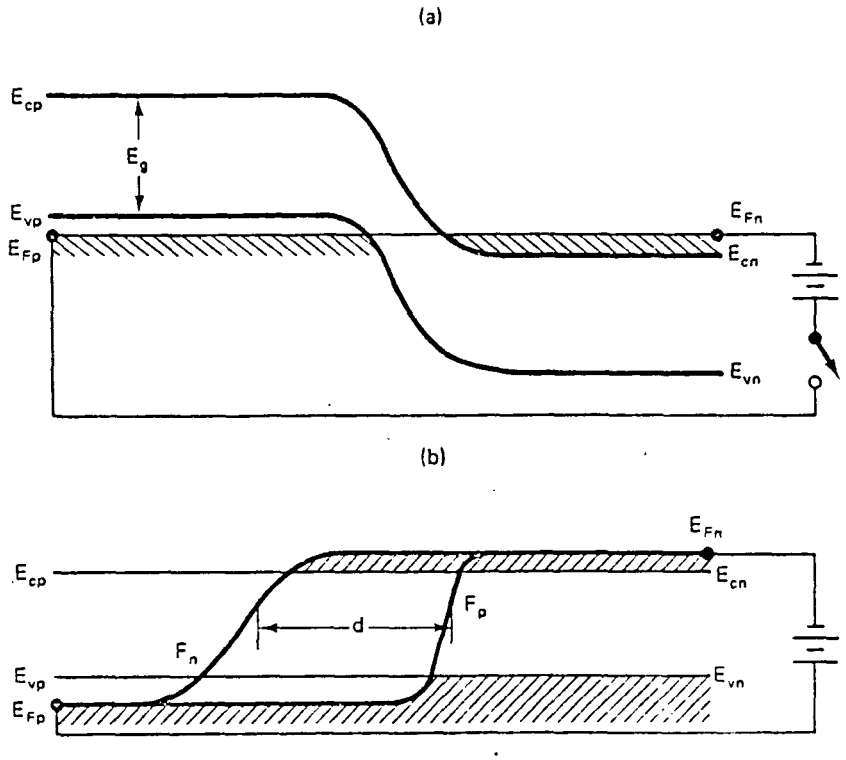

Fig. 3.1 Band diagram of the pn junction(a) at equilibrium (b) with injected current

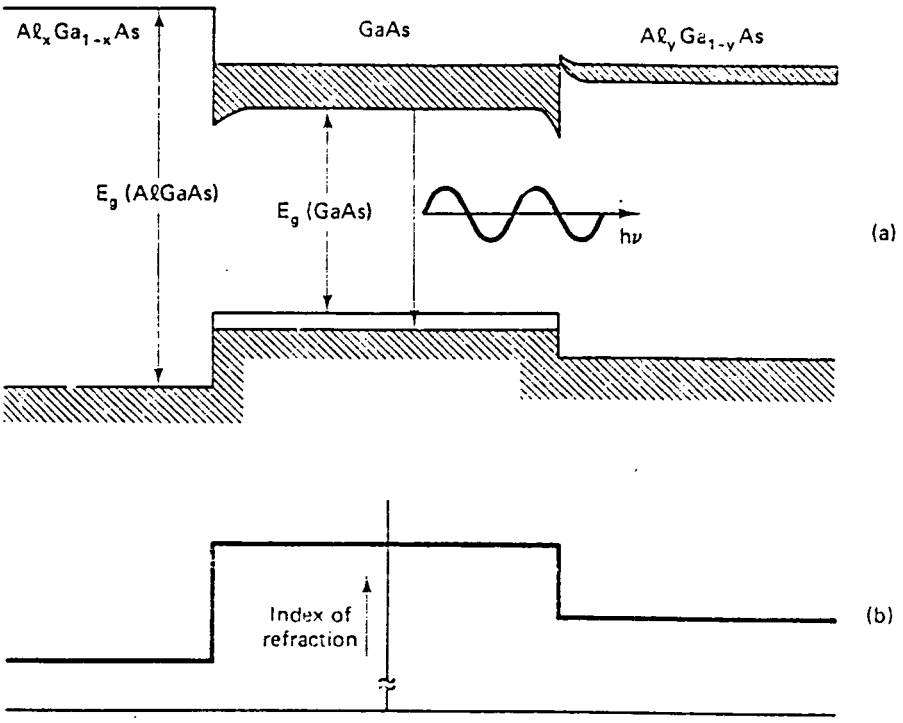

Fig. 3.2 A heterostructure pn junction(a) Band diagram for the forward biased heterostructure (b) the refractive index profile for the heterostructure

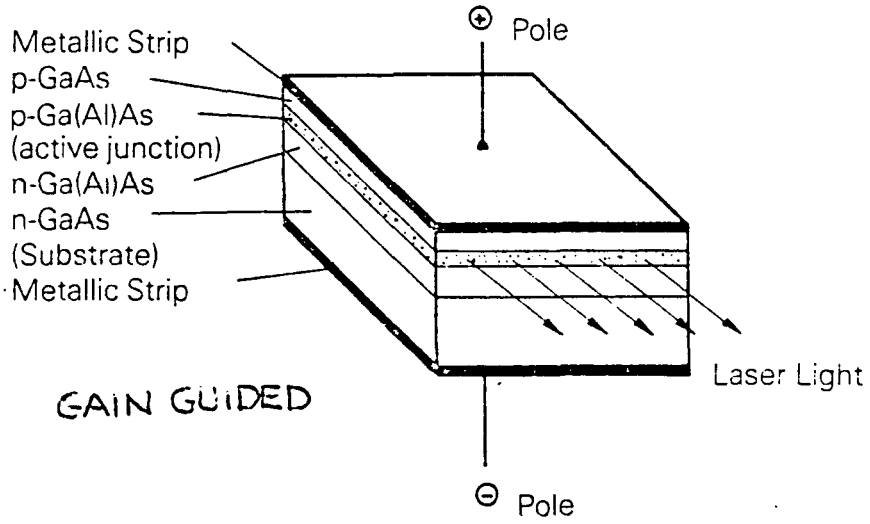

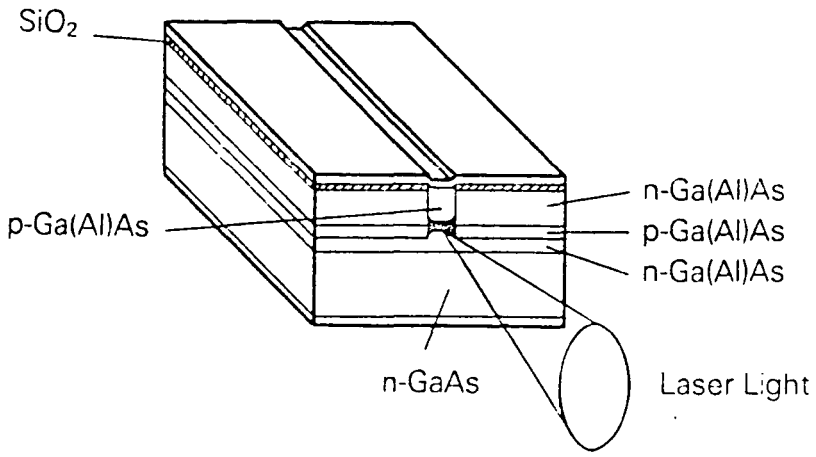

Index guide laser diode

Fig. 3.3 Gain guided laser and index guided laser

refractive index of the semiconductor decreases with an increase in the bandgap. Thus, the refractive index of the active layer is higher than the two surrounding regions and this provides a slab waveguide for optical confinement (see Fig. 3.2b). Various waveguiding mechanisms are available in commercial laser diodes. Most laser diode waveguiding techniques can be separated into two categories: gain-guided lasers and index-guided lasers. For a detailed description of various waveguiding structure, one should consult the most current literature. An example of a gain-guided laser and an index-guided laser (i.e., buried heterostructure) is shown in Fig. 3.3.

3.2 Typical Output Characteristics;

3.2.1 L-I Curve

Fig. 3.4 shows a typical light output versus current characteristic of a GaAs semiconductor laser. The output power starts to increase very rapidly around a threshold current, which roughly represents the beginning of laser oscillation. Very often, the kink in the L-I curve is very smooth, and the smoothness of the kink depends on the rate of effective spontaneous emission in the laser diodes. The L-I curve is very sensitive to temperature change and is shown in Fig. 3.5.

3.2.2 Spectral width of emission

One important characteristic of a laser diode is the spectral width of emission. The spontaneous emission spectrum is usually very broad with a typical width of about 200 to 300 Angstrom. As the laser starts to oscillate, the spectral width narrows down. A spectrum of a

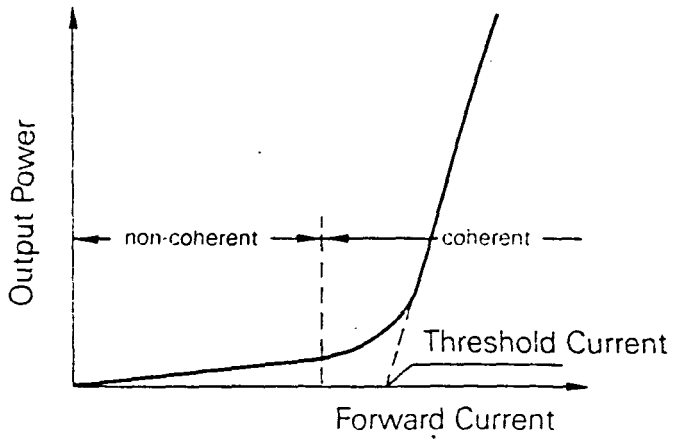

Fig. 3.4 L-I curve of a laser diode

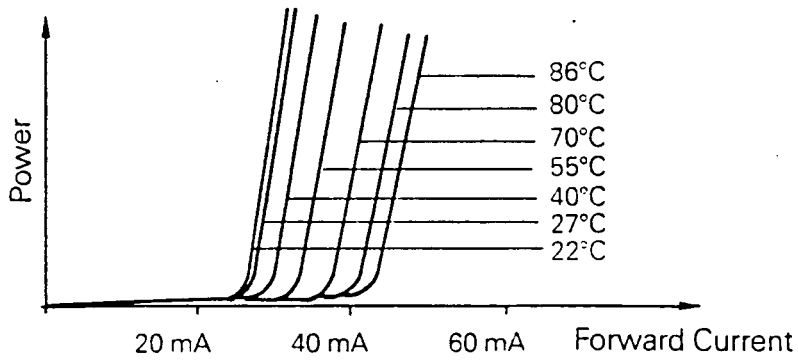

Fig. 3.5 Temperature effect on the L-I curve of a typical gain-guided laser

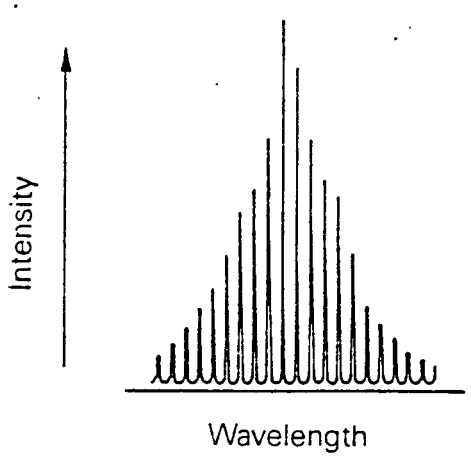

Fig. 3.6 Spectrum of a multimode laser

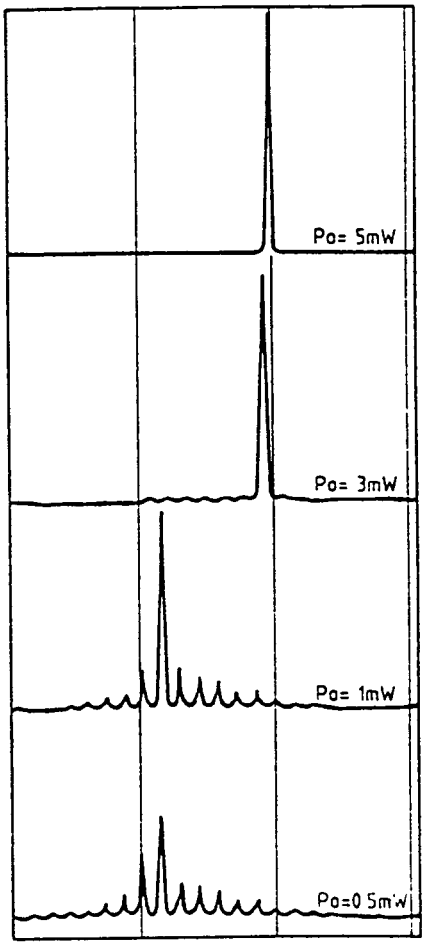

Fig. 3.7 Number of modes dependent on output power

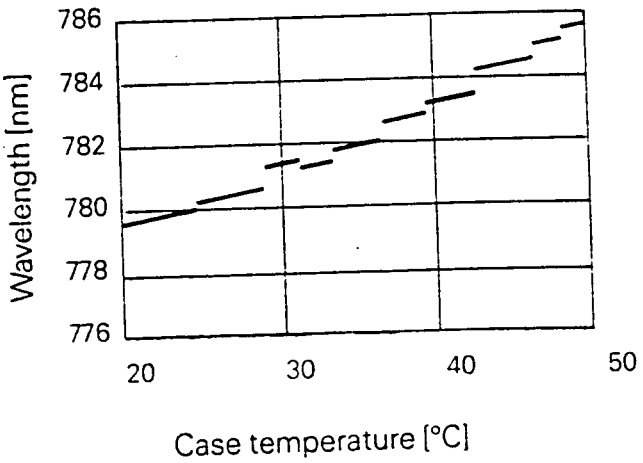

Fig.3.8 Mode hopping of a diode laser

multimode diode laser is shown in **Fig. 3.6.** It should be noted that the mode spacing between various modes is the mode spacing for the laser diode cavity or the resonant cavity as discussed in Chapter 2. The FWHM (i.e., Full Width at Half Maximum of the spectrum) for a multimode laser is around 3 nm. The number of lasing modes decrease as the output power increases as shown in **Fig. 3.7.** This is the result of gain saturation. When the laser is operating in a single mode, the spectral width is less than 1 Angstrom.

3.2.3 Temperature drift

The wavelength of a laser diode increases with rising temperature. Wavelength jumps are known as mode hopping. Between these jumps the wavelength increases linearly with rising temperature. Taking into account mode hopping, the temperature drift of the wavelength is approximately 0.2 nm/degree Celsius. The mode hopping phenomenon is shown in **Fig. 3.8.**

Besides the above characteristics, the performance of laser diodes is being compared in terms of beam divergence, polarization ratio, pulse response and far field radiation pattern. The technical specification of the laser diode being used in this research work is shown in the Appendix.

4. ELEMENTS OF AN OPTICAL MAGNETOMETER

4.1 Review of Current Technology

The applications of magnetic sensor technology are numerous and diverse. For example, the magnetic sensor has obvious applications in the Navy for submarine detection. The magnetometer has also been used for medical diagnostics purposes, in the measurement of mega-ampere plasma currents in fusion devices and in non-destructive evaluation. Currently available magnetometers include a SQUID (Superconductivity Quantum Interference Device), fluxgate and induction probe. Within the past ten years, government laboratories and universities have been studying the possibility of using fiber optic magnetic sensors to replace existing sensors in many applications.

Two types of fiber optic magnetic sensors have been extensively studied - magnetostrictive sensors and Faraday rotation sensors. The fundamental difference between the two sensors is the physical mechanisms on which they are based. The Faraday effect is a linear process involving a direct interaction between the external magnetic field and the light propagating in the core of the fiber. Due to the linear nature of the device, Faraday sensors have been used widely for ac current measurement. The magnetostrictive sensors, on the other hand, utilize a non-linear interaction between the external field and the magnetostrictive material. The resultant distortion of the magnetostrictive material must be transferred to the fiber by physically attaching the fiber to the magnetostrictive material. The non-linear nature of the magnetometer can be used advantageously for signal processing, such as heterodyne detection [7]. **Fig. 4.1** shows the recent research efforts in magnetic sensors. According to current literature, magnetostrictive sensors, based on metallic glass, (e.g., Metglass 2605) and

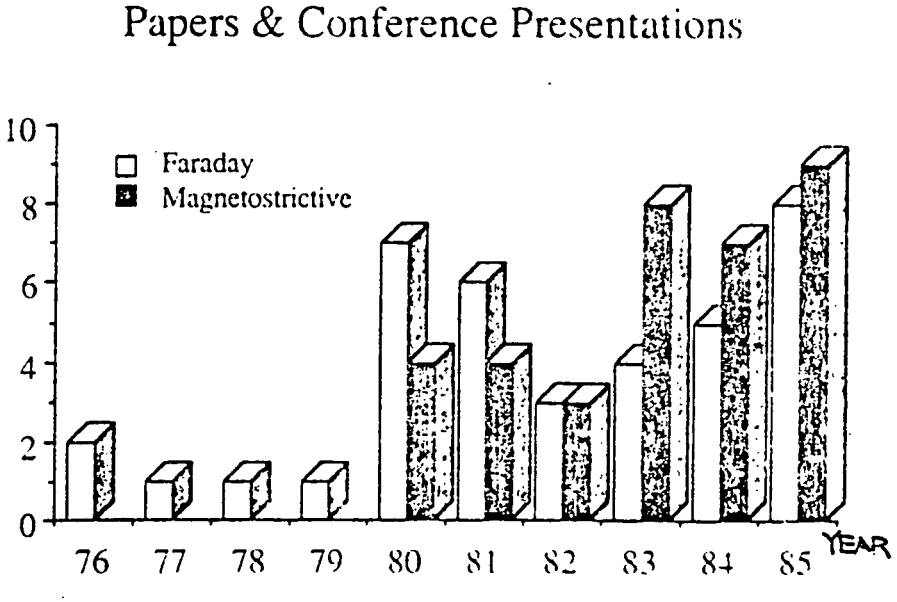

Fig. 4.1 Number of publication and conference presentation for magnetostrictive and Faraday rotation sensor

heterodyne techniques, can measure in the micro-Oersted region. In this research project, the magnetostrictive approach was adopted.

4.2 Magnetostrictive Transducers

The basic principle of a magnetic field transducer is to convert the strength of the magnetic field into a measurable quantity, such as impedance, strain, or voltage. In this research work, a piece of Terfenol-D rod was used as a magnetic field strength to strain transducer. Terfenol-D is a highly magnetostrictive alloy of Terbium-dysprosium-Iron with the chemical formula $Tb_{0.3}Dy_{0.7}Fe_{1.95}$. It is capable of producing over fifty times the strain demonstrated by nickel [8], a well known magnetostrictive element. However, Terfenol-D has a lower relative permeability than nickel and this may make the design of magnetic circuits more difficult. In addition, Terfenol-D requires a dc bias field for optimum performance. The magnitude of this bias field is about six to seven times higher than for nickel. However, Terfenol-D demonstrates some unique features which cannot be found in conventional magnetostrictive materials. For example, Terfenol-D has an extremely high saturation magnetostriction at around 1200 ppm under no stress and increases to about 2000 ppm under a compressive stress of 2.0 ksi, which is shown in Fig. 4.2 and Fig. 4.3. Also, the differential (i.e., small signal) magnetostriction of Terfenol-D varies from 4.2 ppm/Oe to a maximum of 10.8 ppm/Oe under a compressive stress of 0 ksi and 1.1 ksi respectively (see Fig. 4.4). Consequently, Terfenol-D offers the possibility of varying its sensitivity to magnetic field strength by adjusting the compressive stress magnitude. However, it should be noted that slightly different bias fields are needed for Terfenol-D to operate at its optimum point under different stress conditions. This is demonstrated in Fig.4.5 [9]. Although Terfenol-D demonstrates hystersis in its B-H curve, the ac performance of the transducer is

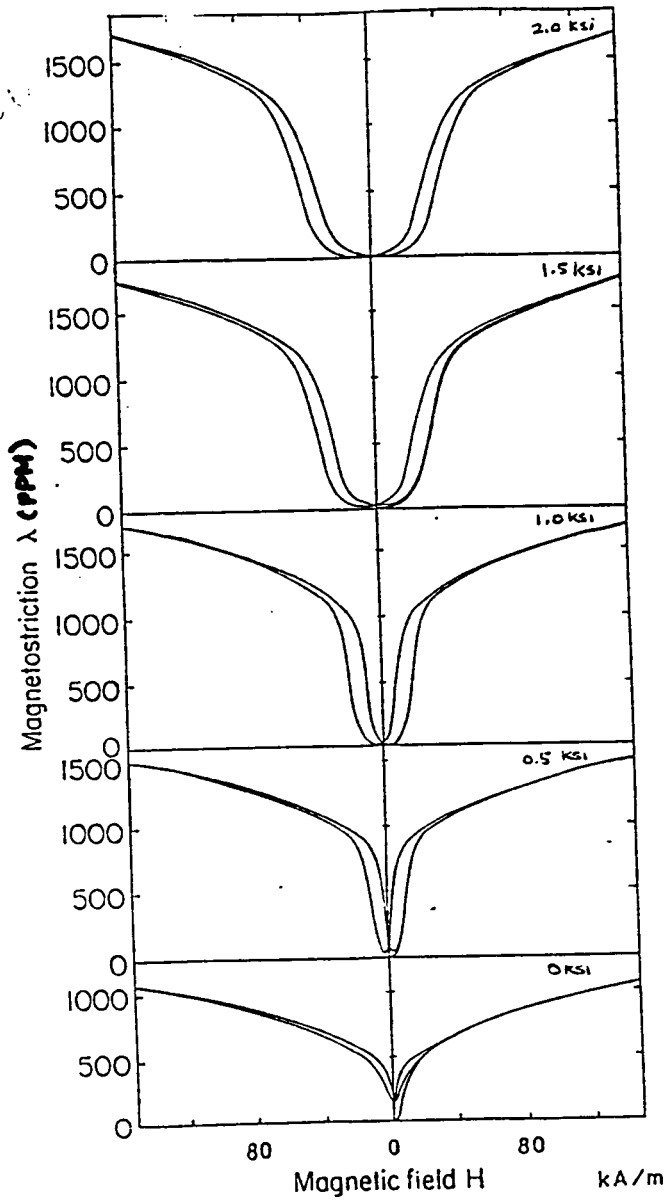

Fig. 4.2 Magnetostriction in ppm as a function of magnetic induction for different level of stress

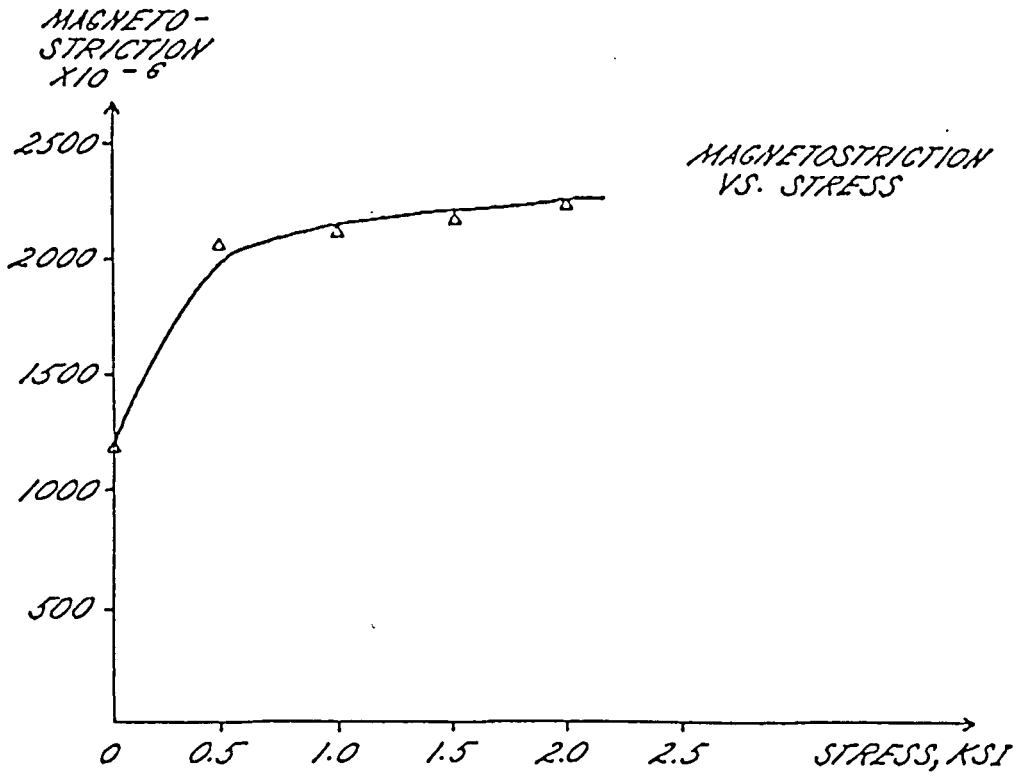

Fig. 4.3 Maximum saturation magnetostriction as a function of stress at 3.0 kOe

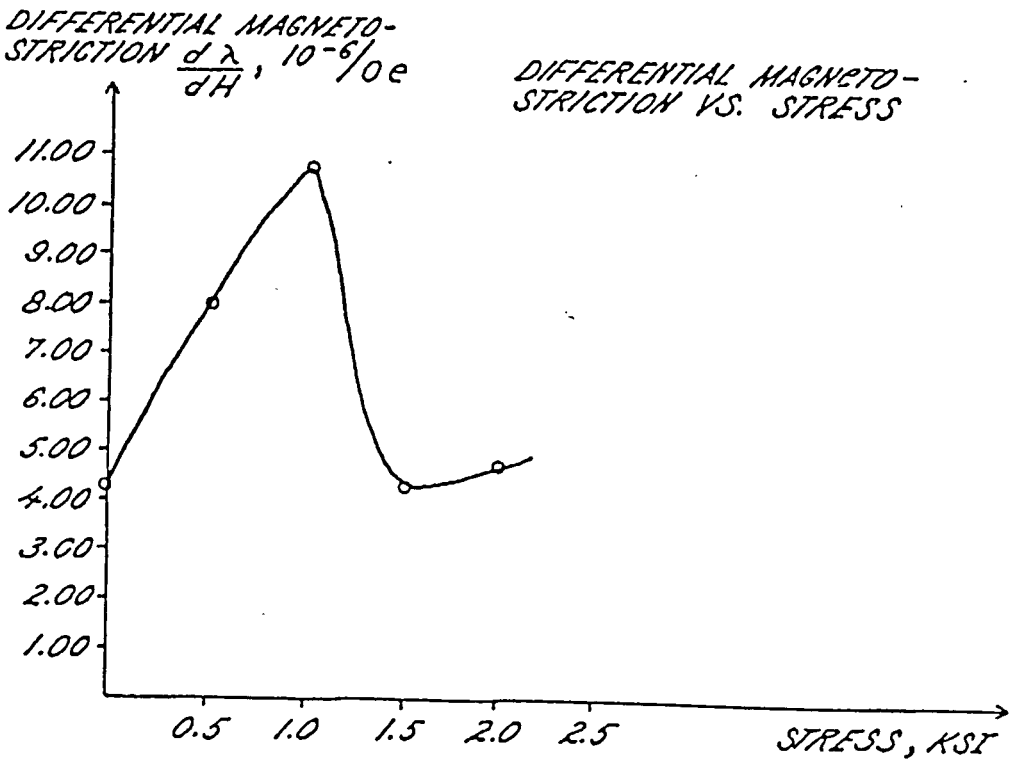

Fig. 4.4 Maxmium differential magnetostriction as a function of stress

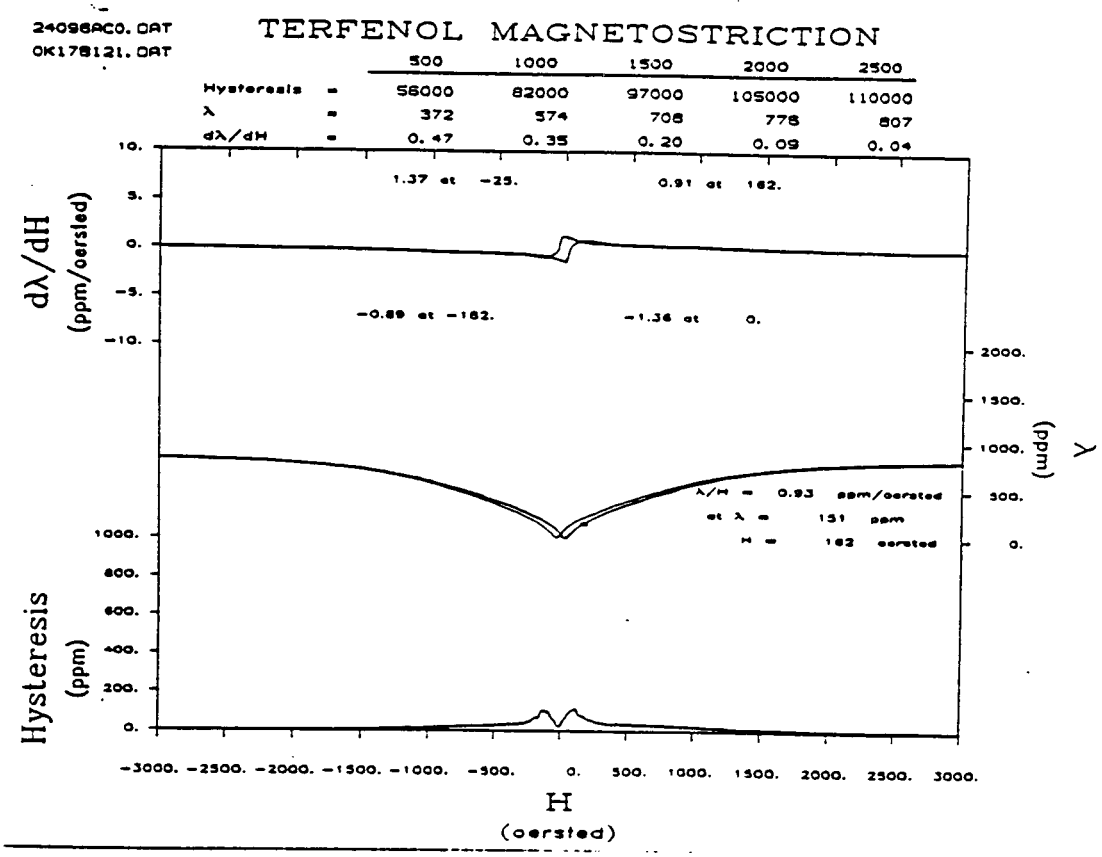

Fig. 4.5a Terfenol magnetostriction under various stress and optimum bias points at 0 ksi [9]

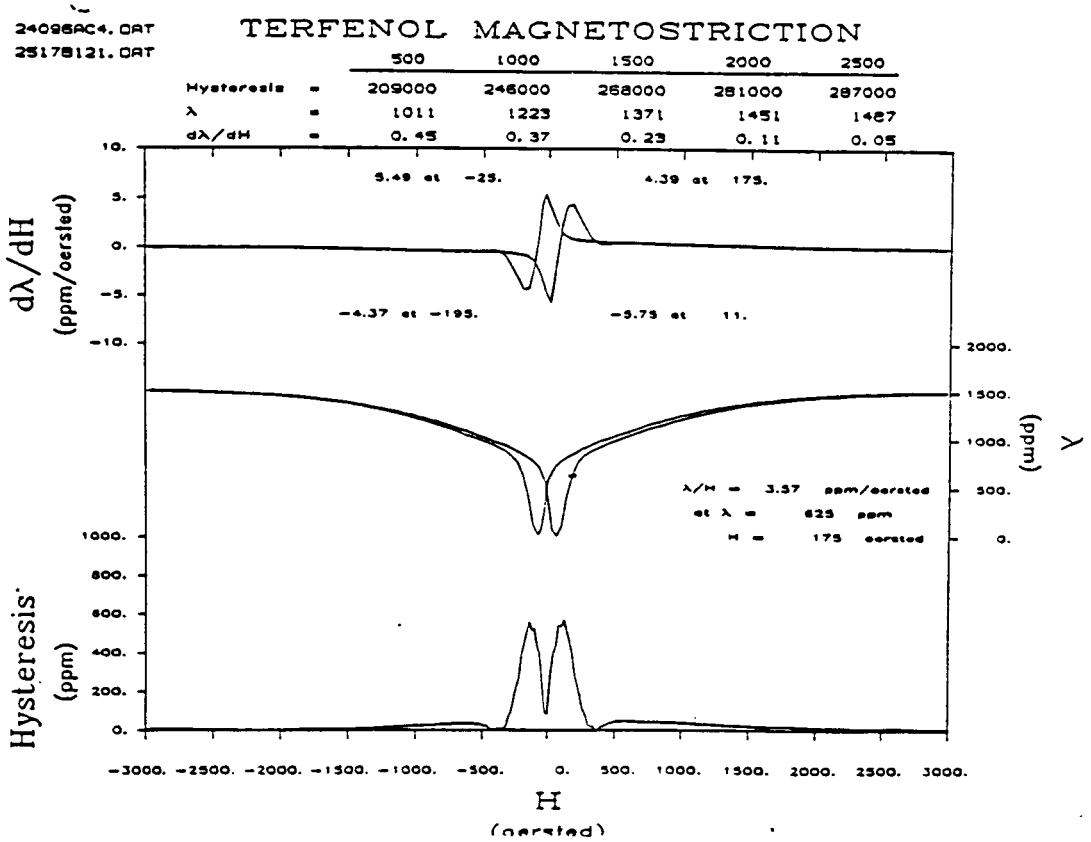

Fig. 4.5b Terfenol magnetostriction under various stress and optimum bias points at 0.25 ksi [9]

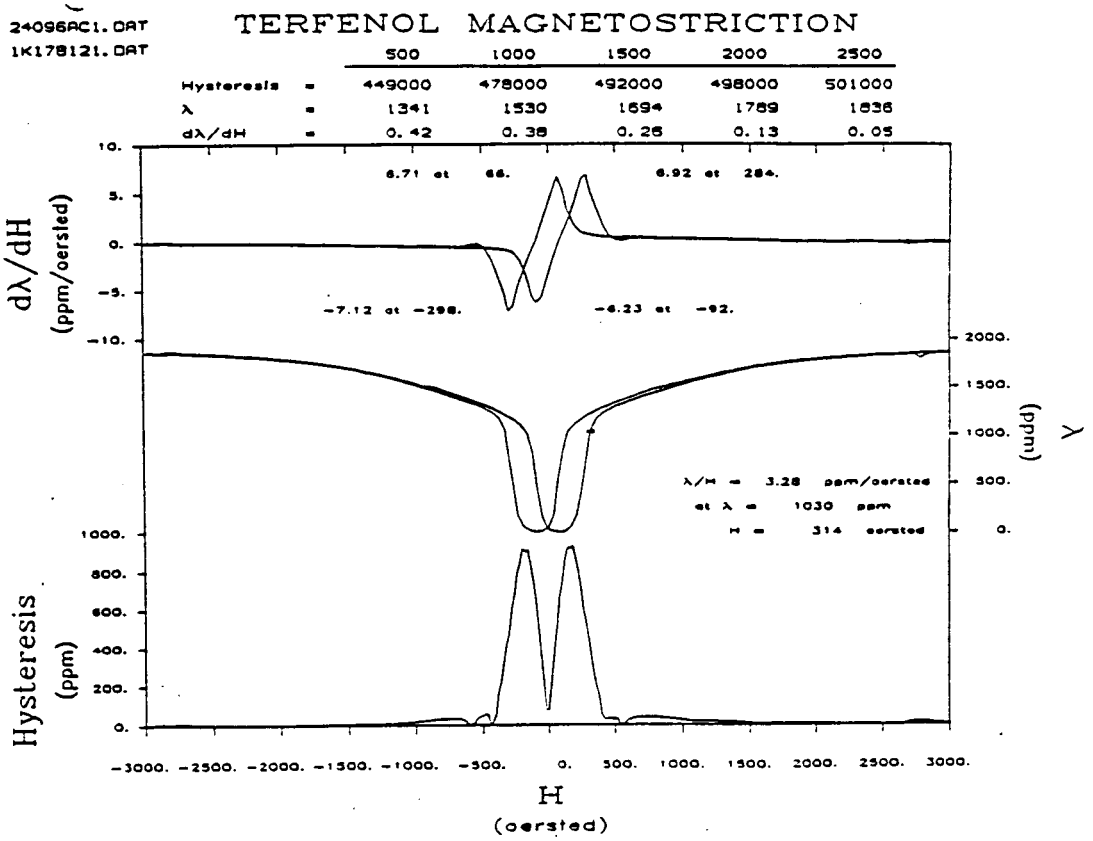

Fig. 4.5c Terfenol magnetostriction under various stress and optimum bias points at 1.00 ksi [9]

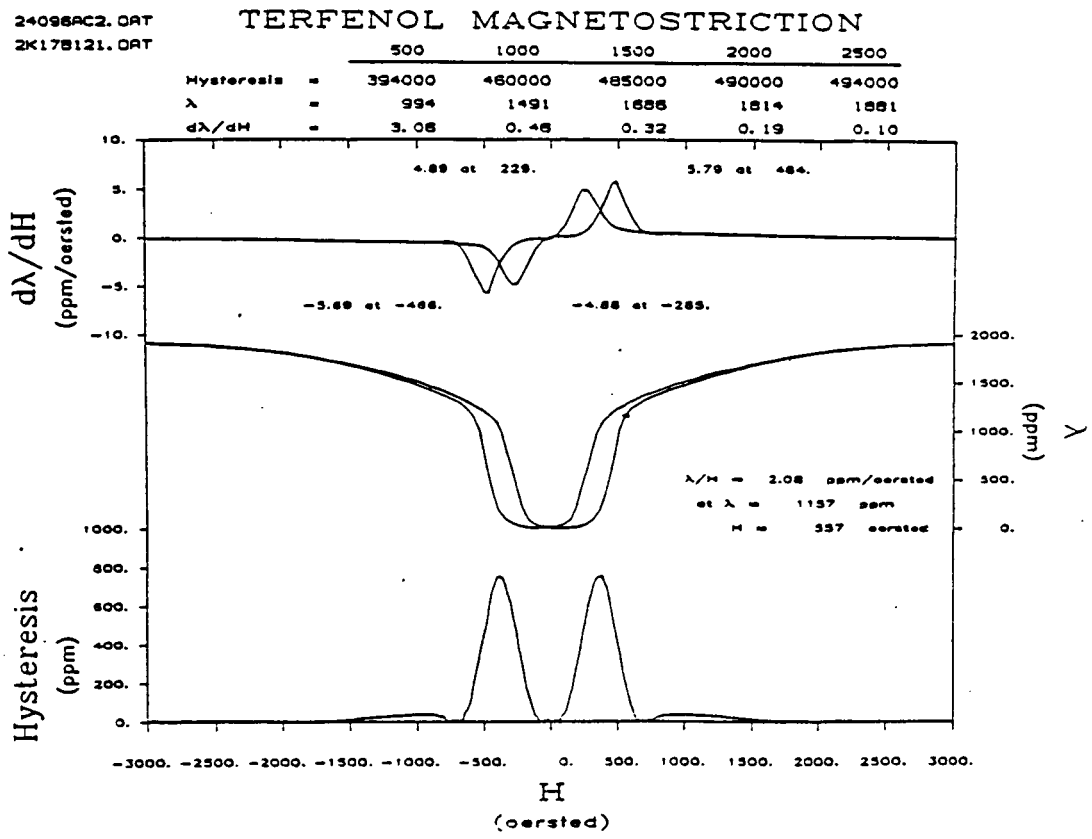

Fig. 4.5d Terfenol magnetostriction under various stress and optimum bias points at 2.00 ksi [9]

not affected. Since the information of the magnetic field intensity is given by the peak to peak amplitude of the magnetostriction, which is not dependent on the hystersis history.

4.3 Short External Cavity Laser Diode Sensor

Fiber optic sensors have demonstrated high sensitivity [10] in magnetic field measurements. However, they are only limited to laboratory applications due to their complexity. Therefore, fiber optic sensors are unattractive for applications that require a simple, rugged, miniature but relatively sensitive device. Short external cavity laser diode sensors or simply diode sensors, however, seem to be a perfect candidate for such applications. A diode sensor is a phase sensing device , which has demonstrated a minimum detectable phase shift of 10 micro-radian at 70 Hz and a phase shift of 1 micro-radian at 1 KHz. [11]. Moreover, diode sensors are packagable into a small device. The sensor also has the advantage of being very simple and relatively cheap. In this research work, a compact-disk player type laser diode, lasing at 0.78 micrometer was used. Fig. 4.6 shows the experimental arrangement of the diode sensor. The sensor consists of a laser diode operating in a cw mode and an external reflector. The position of the reflector was modulated by a transducer. In this research work, the Terfenol-D rod became the transducer. The output signal was obtained by the photodetector, which was included in the same package as the laser diode in this research work. The external reflector feeds light back to the laser cavity and perturbs the operation of the diode laser. When the light is fed back in phase with the light in the semiconductor laser cavity, the effective reflectivity of the facet facing the reflector is raised. Conversely, when the light is fed back out of phase, the effective facet reflectivity is lowered. This change in facet reflectivity was reflected in the power output of the laser diode under a constant bias condition. It should be noted that the phase of the light was determined

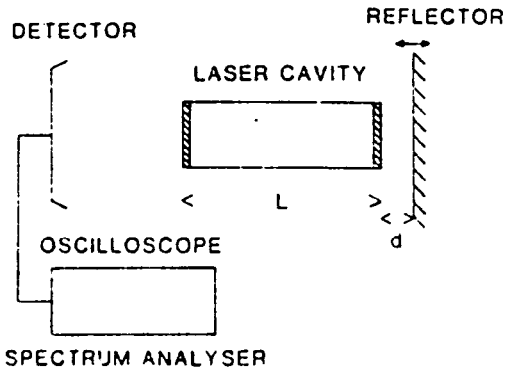

Fig. 4.6 Experimental arrangement of the diode laser sensor

by the distance between the reflector and the laser facet and by the reflection coefficient of the reflector. Furthermore, the sensing scheme achieved its best performance for a short external cavity (i.e., less than 10 micrometer), which was formed by the laser facet and the external reflector.

4.4 Supporting Electronics and Components

The critical elements of the magnetometer were discussed in the previous context. In addition to the magnetic field transducer and the sensor, some auxiliary equipment was needed. For example, in biasing the laser diode, a power supply with soft turn-on and turn-off features is required. Also, to make sure the laser diode is not overheated, a Peltier device was used. Moreover, some means of producing a dc bias field for the transducer was needed. A solenoid was being used to generate the magnetic field. Furthermore, some signal processing electronics such as an averaging scope and filters were needed to enhance the signal-to-noise ratio.

5. IMPLEMENTATION AND EVALUATION OF THE LASER DIODE MAGNETOSTRICTIVE TERFENOL-D MAGNETOMETER PROTOTYPE

The necessary components for fabricating the magnetostrictive magnetic sensors were discussed in the previous chapter. The detail of the implementation and preliminary testing which resulted is presented in the following section.

5.1 Implementation of the Magnetometer

The first step in fabricating the magnetometer was to remove the encapsulation of the laser diode package to allow the formation of a short external cavity. The second step involved the polishing of the Terfenol-D rod end surface to perform the function of the external reflector. The polishing work is very important since a bad reflector will scatter the laser beam, and the diode will not operate as a sensor. The Terfenol-D rod was polished with 10 micrometer, 9 micrometer, 5 micrometer, 3 micrometer and 1 micrometer fiber optic grade sandpapers. The quality of the polished surface was checked by shining a laser beam onto the surface and observing the diffraction pattern under a microscope. The third step involved the machining of the housing for the prototype. The cross-section view of the housing is shown in **Fig. 5.1.** An important point in the housing is the cylindrical compartment for the Terfenol-D rod. The compartment was made such that the rod was free to slide and still kept the longitudinal axis of the Terfenol-D rod coinciding with the axis of the laser beam. Also, one end of the Terfenol-D rod was fixed with respect to the housing and the other end was free to move. Furthermore, the housing was equipped with a screw to fine tune the position of the distance between the end surface of the rod and the laser facet (see **Fig. 5.1**). Finally,

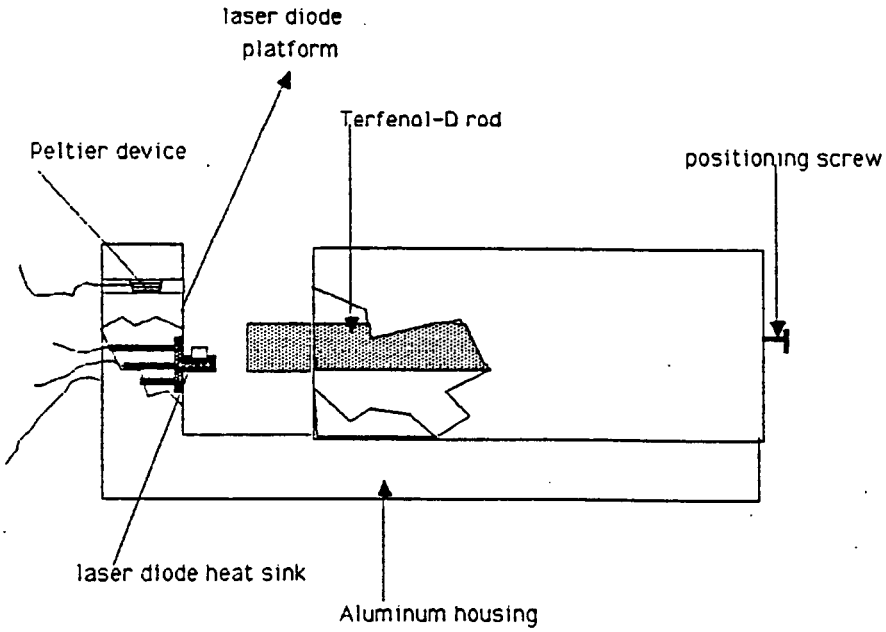

Fig. 5.1 Magnetometer housing

the Peltier device was incorporated into the laser diode platform (see Fig. 5.1). After the diode was wired properly, the entire housing was inserted into a solenoid, which provided the dc bias field, for evaluation.

5.2 Evaluation of the Prototype

To evaluate the prototype properly and precisely, one should examine both the laser diode sensor and the Terfenol-D rod. However, the evaluation of the laser diode sensor required a displacement device, such as a piezoelectric positioner or a stepper motor positioner, having a resolution of 0.1 micrometer or less. Since this was not available in Electrical Engineering and Computer Engineering's microwave laboratory, the testing of the laser diode sensor was carried out in the 'Optics and Thermal Wave Laboratory' of the NDE center using a x-y-z positioner with 1 micrometer resolution. However, such a positioner was still found to be inadequate. Special techniques were used and these will be discussed later.

5.3 Operation of Laser Diode with Feedback

The de-encapsulated laser diode was studied under a microscope, and is shown in Fig. 5.2 and a blown-up view is shown in Fig. 5.3. One very important point, which is critical to the diode sensor operation, was observed. As shown in Fig. 5.3, the laser diode package consists of a header, a low-cost photodetector, a heat sink, three connecting pins, and a laser chip. A close examination of the diode under the microscope indicated that the laser chip and the heat sink are not aligned. Some examples of these problems are shown in Fig. 5.4. The lateral offset of the laser chip and the edge of the heat sink may be 50 micrometer, which severely degrades the sensitivity of this device. Also, when the prototype housing was

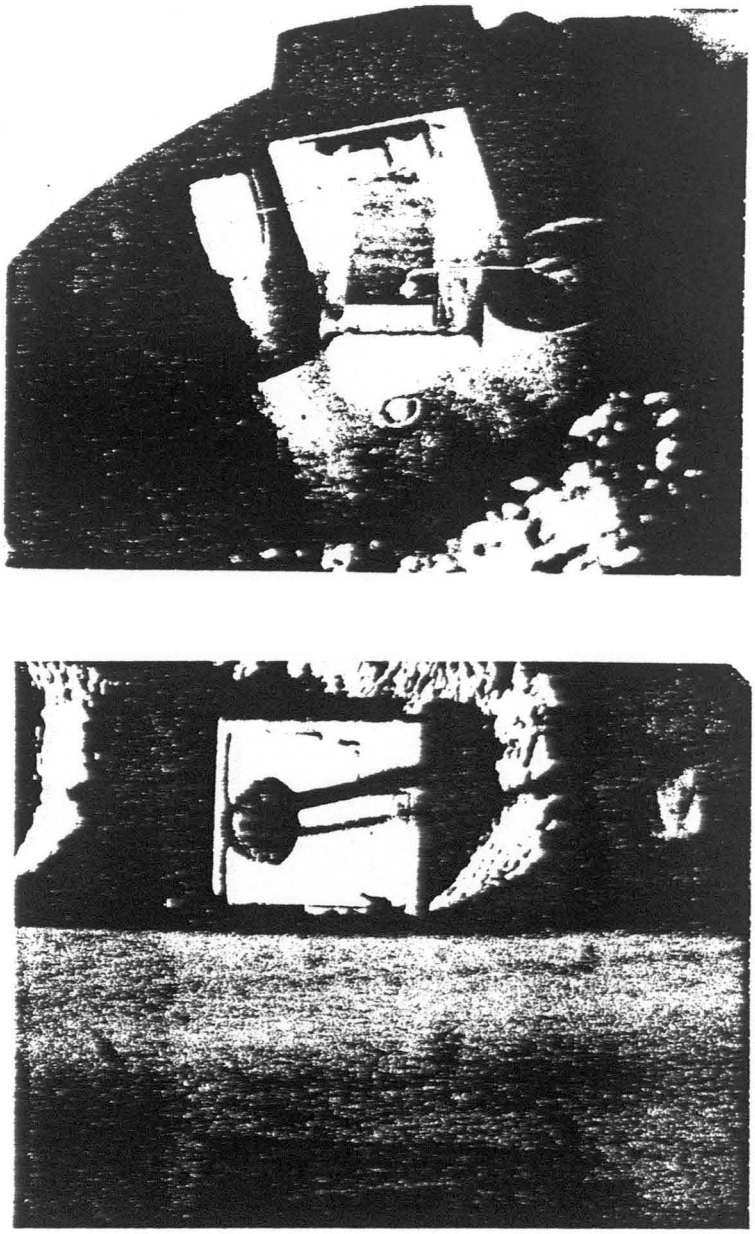

Fig. 5.2 De-encapsulated laser diode seen under a microscope

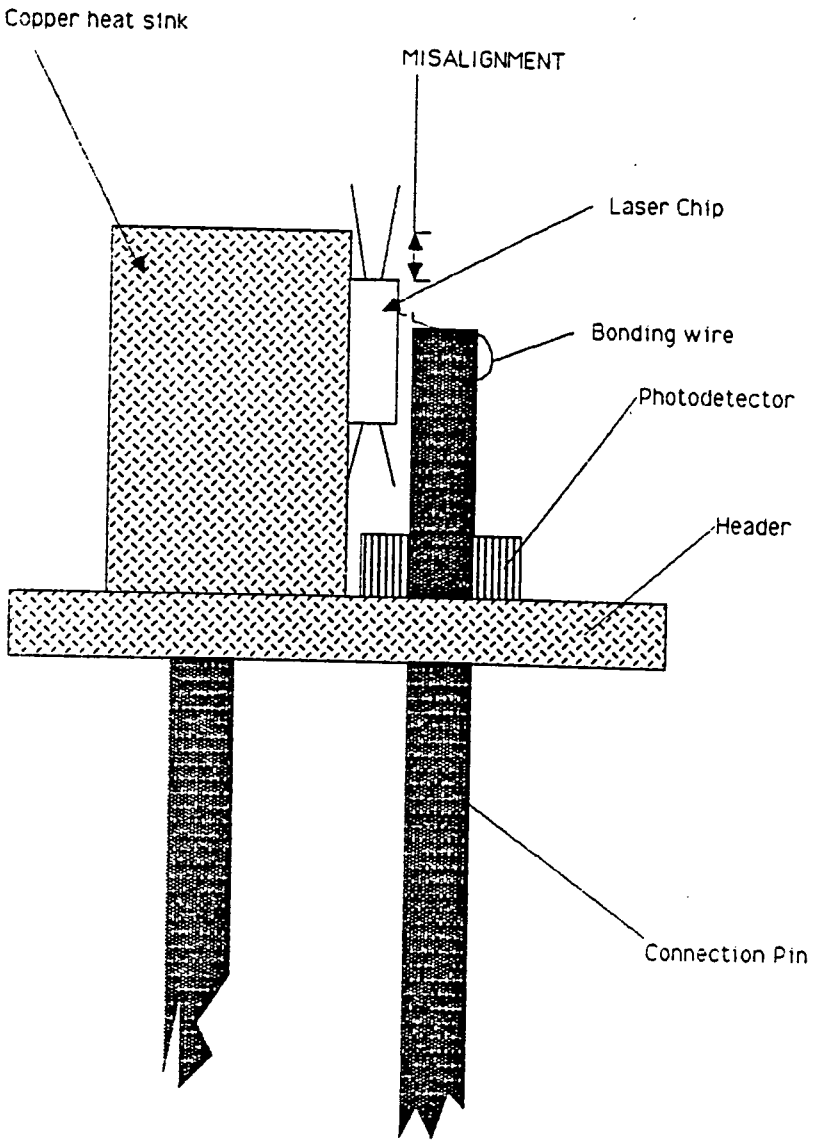

Fig. 5.3 A blow-up view of the decapsulated laser diode

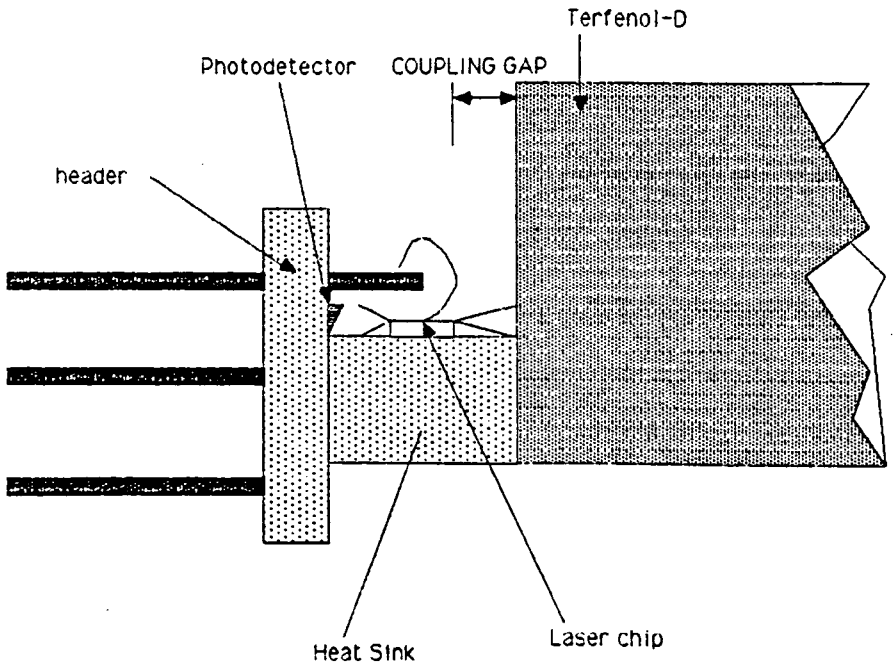

Fig. 5.4 An example of a coupling problem resulted from imperfect diode alignment

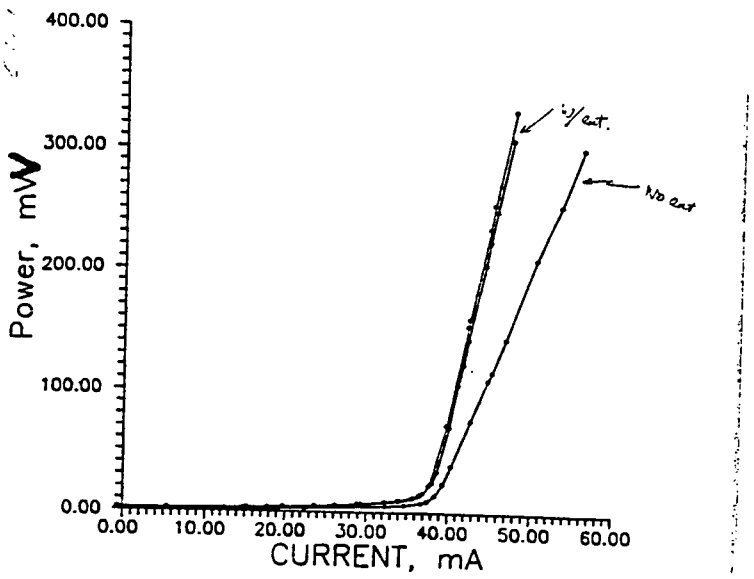

Fig. 5.5 L-I characteristics of the laser diode with external cavity

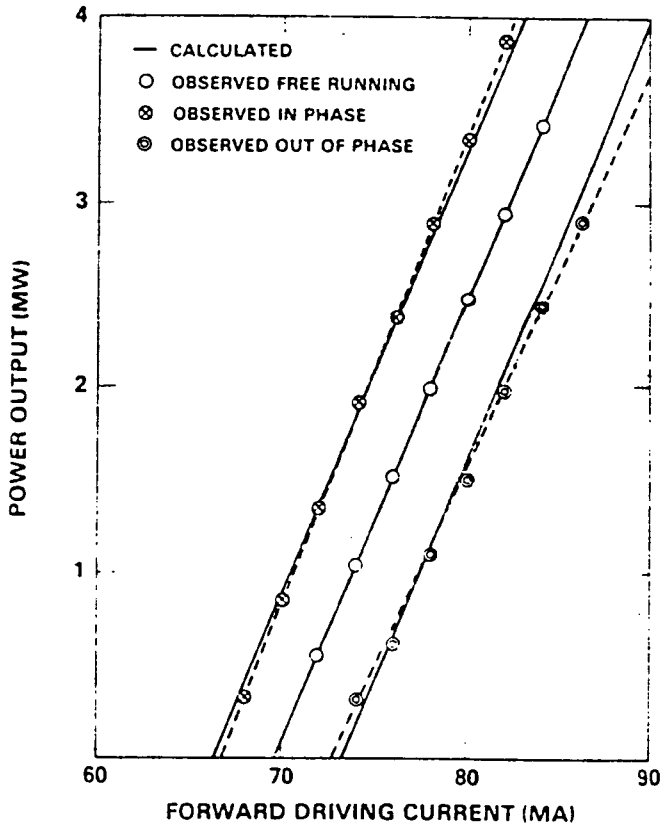

Fig. 5.6 L-I characteristics of the laser diode with external cavity published by reference [11]

designed, this effect was not known. Therefore, the minimum coupling distance is limited by the offset distance from the edge of the heat sink which prevents the Terfenol-D rod from close coupling with the laser facet (see Fig. 5.4). The L-I curve of the laser diode under the influence of the external cavity formed by the Terfenol-D end surface is shown in Fig. 5.5. The L-I curve of the laser diode shifts to the right hand side accompanied with a change in the slope. According to literature [11], this corresponds to light fed back in phase. Similarly, a corresponding out-of-phase condition should be observed as shown in Fig. 5.6. It should be mentioned that the in-phase and out-of-phase condition differs by only half a wavelength (i.e., 390 nm). In addition, the fine positioning screw was not capable of providing a resolution down to the desired accuracy. Therefore, it was necessary to keep repeating the experiment by randomly positioning the Terfenol-D rod looking for in-phase and out-of-phase conditions. However, the out-of-phase condition could not be found.

5.4 Evaluation of the Terfenol-D Rod

The Terfenol-D rod was evaluated with a heterodyne HeNe laser interferometer from the Optics and Thermal Wave Laboratory of NDE center by Mr. Jin-Yong Kim. The experimental setup is shown in Fig. 5.7. The solenoid was driven at 1.4 KHz to produce a magnetic field intensity of 1 Oe. The dc bias was adjusted until the response was maximum. The optimum bias field was found to be 183.6 Oe, which was close to the calculated result [12]. Although the operating frequency of the device was 60 Hz, evaluating the Terfenol at 1.4 kHz approximates the response in the line frequency operation. The main reason for using such a frequency was to allow the PLL in the demodulation circuit of the interferometer to function properly. The result of this measurement is shown in Fig. 5.8.

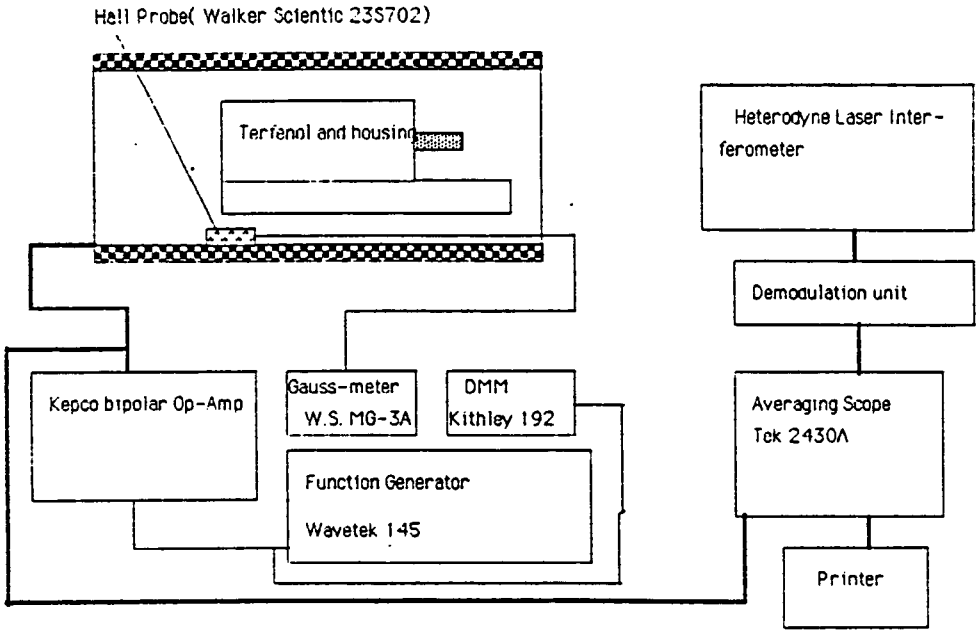

Fig. 5.7 Experimental setup for evaluating Terfenol movement with a heterodyne interferometer

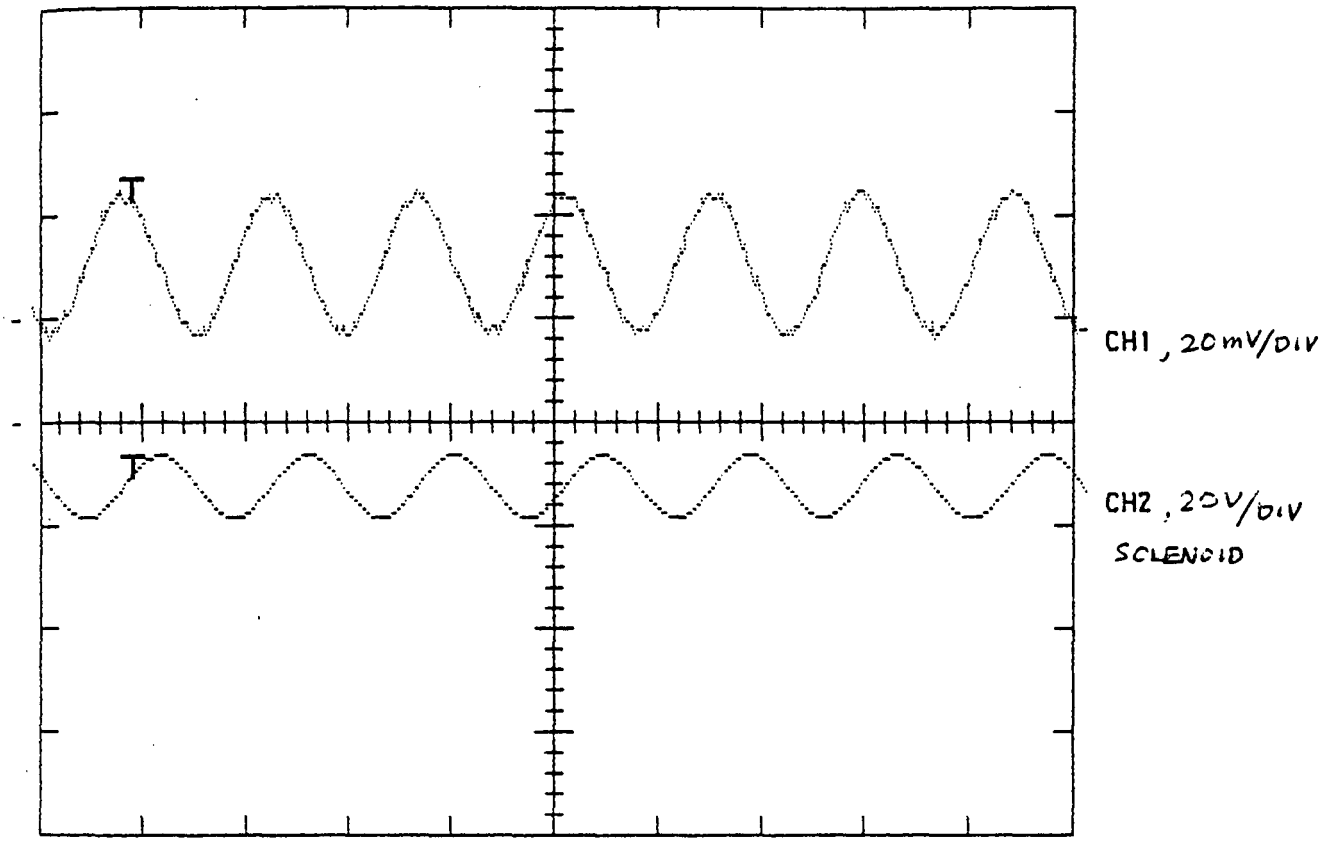

Fig. 5.8 Plot of Interferometer output (calibrated at 0.47 Angstrom/mV) at Ch. 1 and solenoid driving voltage at Ch. 2

5.5 Evaluation of the Magnetometer

After the laser diode and the Terfenol-D rod were examined, the magnetometer was evaluated. The experiment setup is shown in Fig. 5.9. The prototype was evaluated under various conditions: a.) 5 Oe at 90Hz with dc bias at around 183 Oe and the laser diode bias at 62.8 mA (see Fig. 5.10), b.) same as 1 with laser diode bias at 52.2 mA (see Fig. 5.11), c.) same as 1 with laser diode bias at 50.9 mA (see Fig. 5.12), d.) 1 Oe at 90 Hz with dc bias same as 1 and laser diode bias at 60.2 mA (see Fig. 5.13). It should be noted that a waveform distortion was observed in one of the above experiments. No theoretical explanation can be offered at this point. Also, the response of the magnetometer under different dc magnetic field intensities were observed. The laser diode was biased at 43.77 mA, the frequency of the ac magnetic field was at 10 Hz, and the dc bias field was changed from 225.7 Oe to 246.1 Oe. As the dc bias was changed from 225.7 Oe to 246.1 Oe, waveform distortion was observed. The results are shown in Fig. 5.14 and Fig. 5.15, respectively. Also, a very serious waveform distortion was obtained during the experiment by increasing the ac magnitude of the testing field, and is shown in Fig. 5.16. Judging from the above experimental results (i.e., Fig. 5.10-16), one can conclude that the dc bias, the ac field and the laser diode bias current can induce distortion. However, no explanation can be offered at this time due to the complex operating principle, which is discussed in Section 5.7, of the diode sensors.

5.6 Evaluation of the Solenoid

The inductance and capacitance of the solenoid are altered by the incorporation of the magnetometer into its core. This concern was studied with an impedance analyzer and the

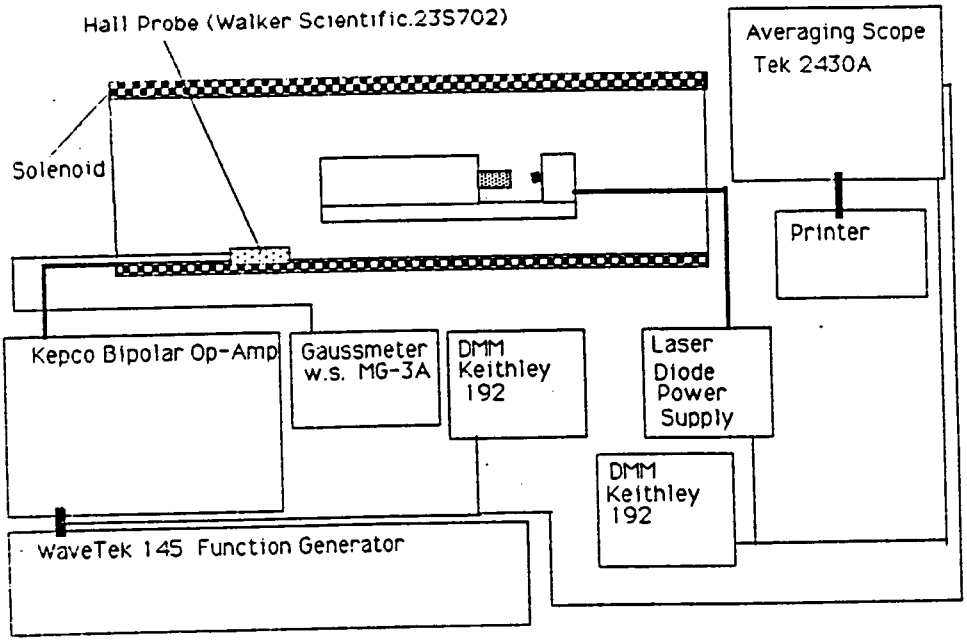

Fig. 5.9 Magnetometer evaluation experiment setup

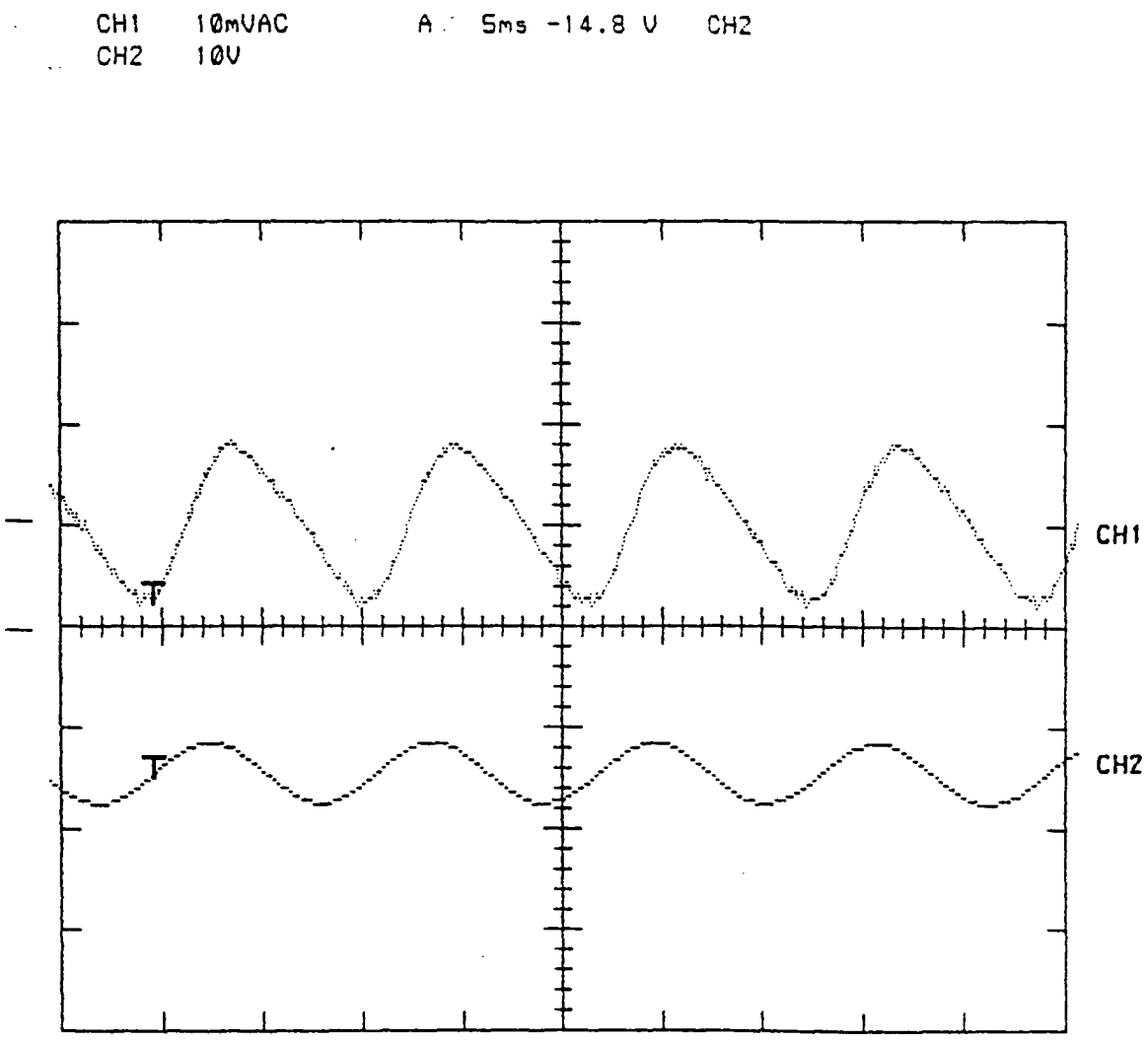

Fig. 5.10 Plot of photodetector voltage at Ch. 1 and solenoid driving voltage at Ch. 2 (with 5 Oe ac field at 90 Hz and a dc bias of 183 Oe, laser diode bias at 62.8 mA)

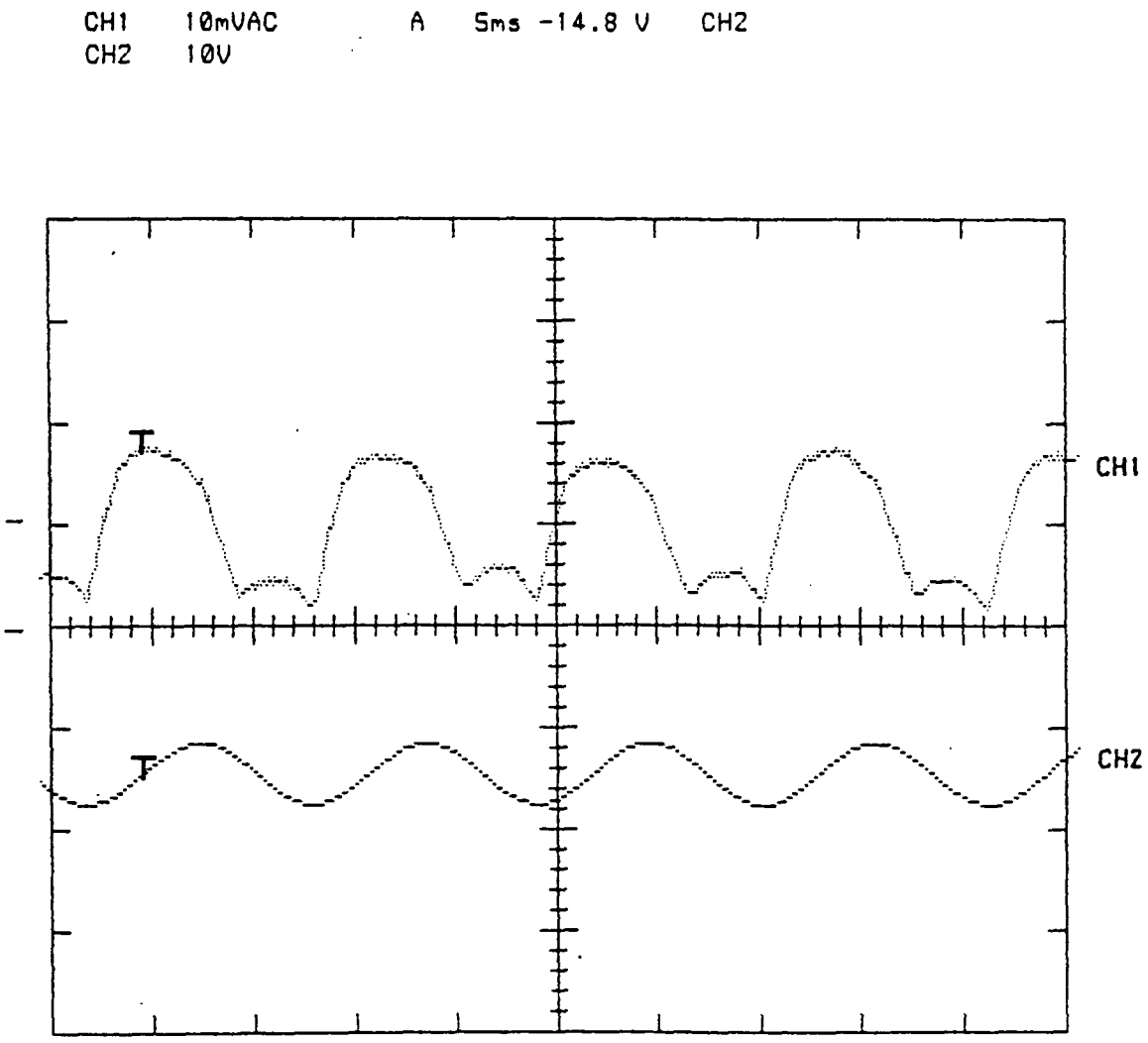

Fig. 5.11 Plot of photodetector voltage at Ch. 1 and solenoid driving voltage at Ch. 2 (with 5 Oe ac field at 90 Hz and a dc bias of 183 Oe, laser diode bias at 52.2 mA)

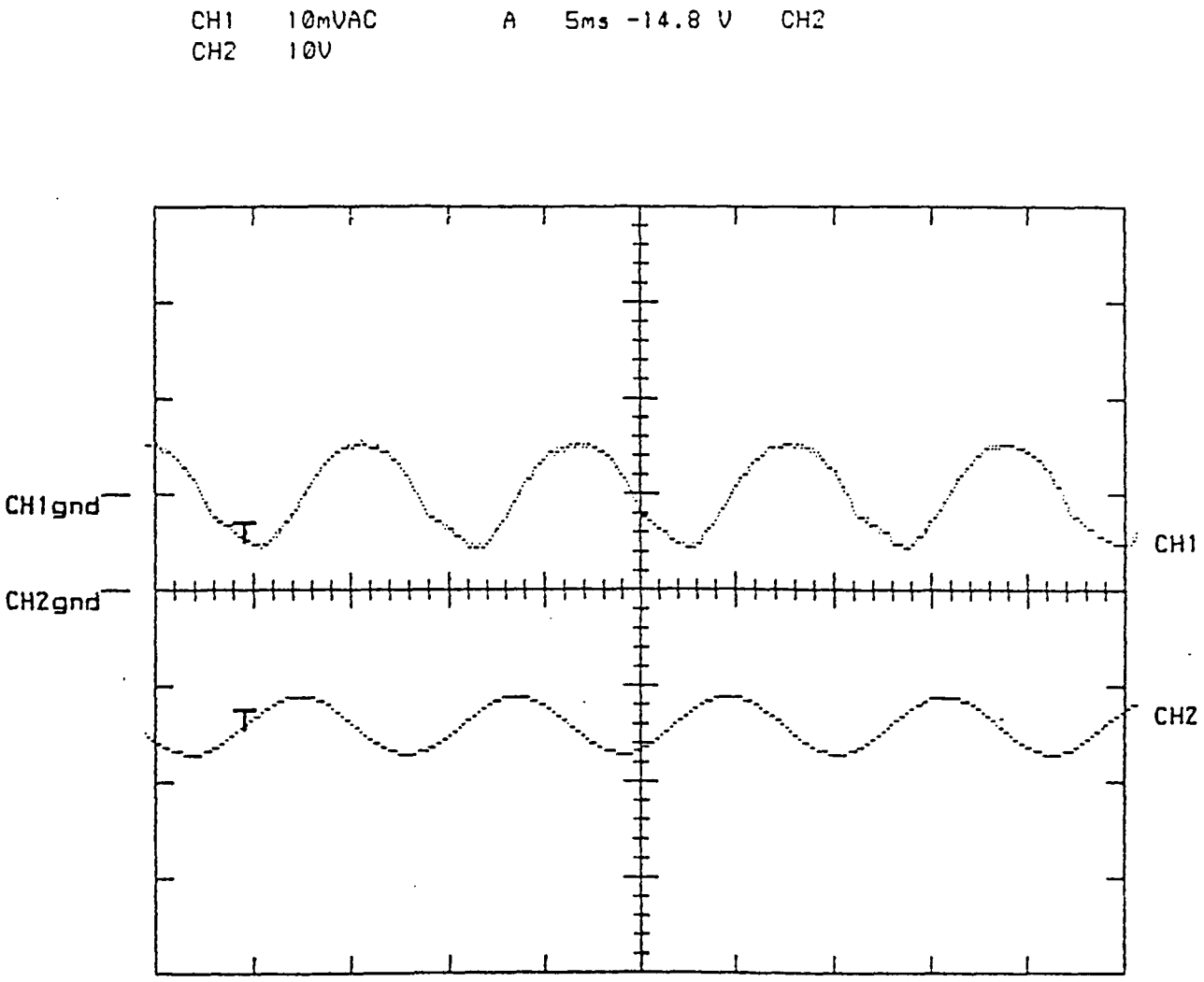

Fig. 5.12 Plot of photodetector voltage at Ch. 1 and solenoid driving voltage at Ch. 2 (with 5 Oe ac field at 90 Hz and a dc bias of 183 Oe, laser diode bias at 50.9 mA)

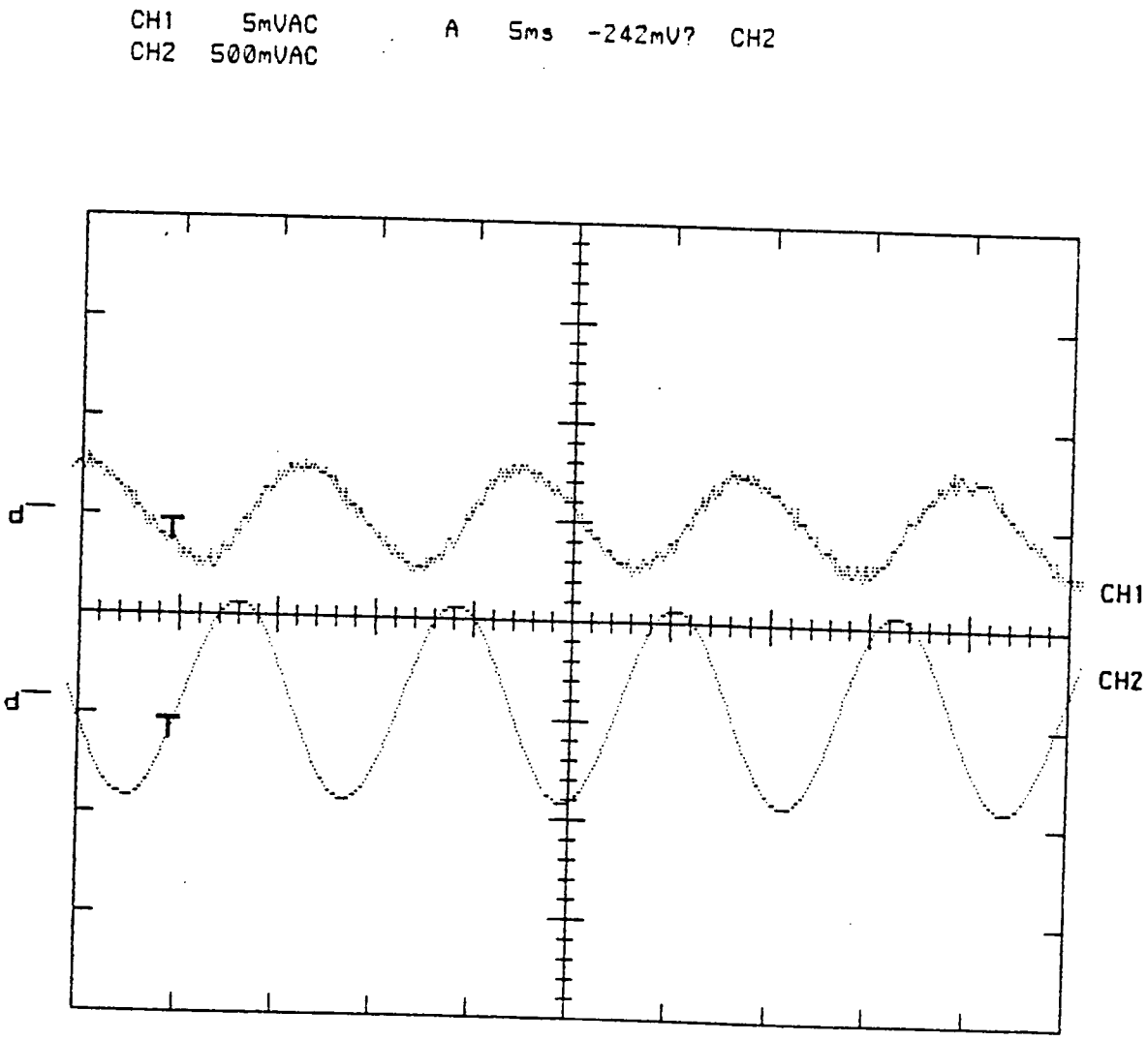

Fig. 5.13 Plot of photodetector voltage at Ch. 1 and solenoid driving voltage at Ch. 2 (with 1 Oe at 90 Hz and a dc bias of 183 Oe, laser diode bias at 60.2 mA)

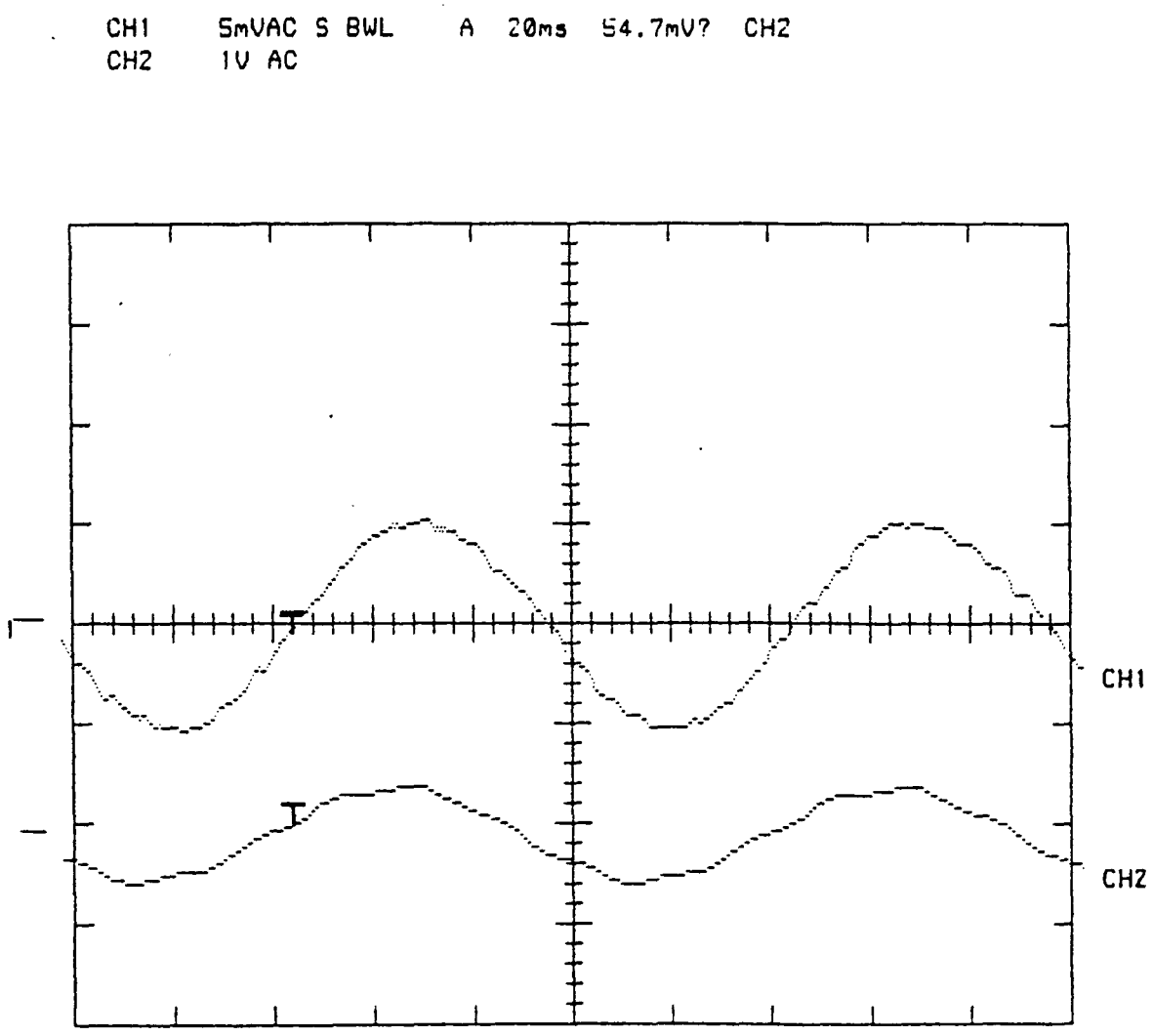

Fig. 5.14 Plot of photodetector voltage at Ch. 1 and solenoid driving voltage at Ch. 2 (at a dc bias of 225.7 Oe)

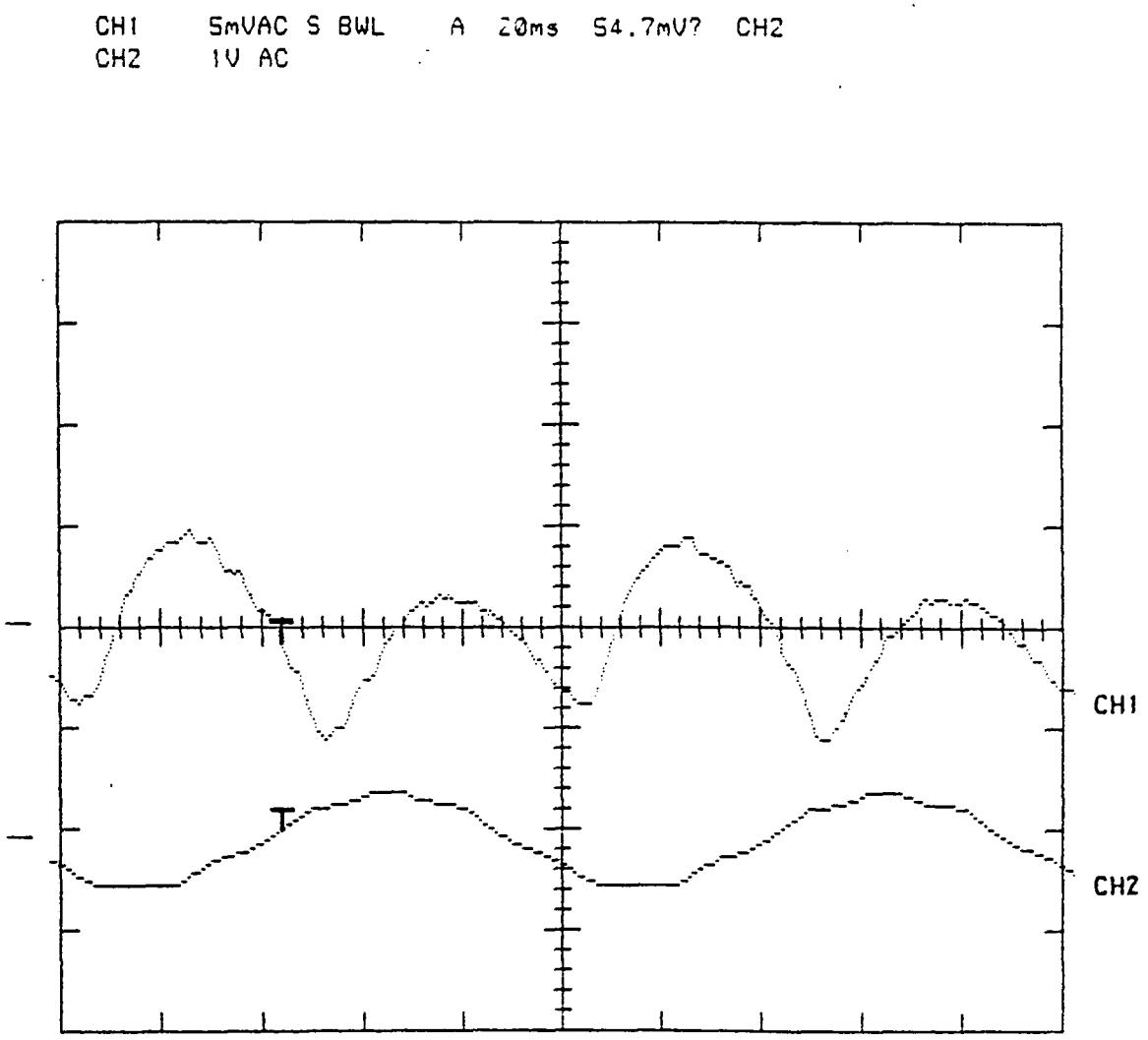

Fig. 5.15 Plot of photodetector voltage at Ch. 1 and solenoid driving voltage at Ch. 2 (at a dc bias of 246.1 Oe)

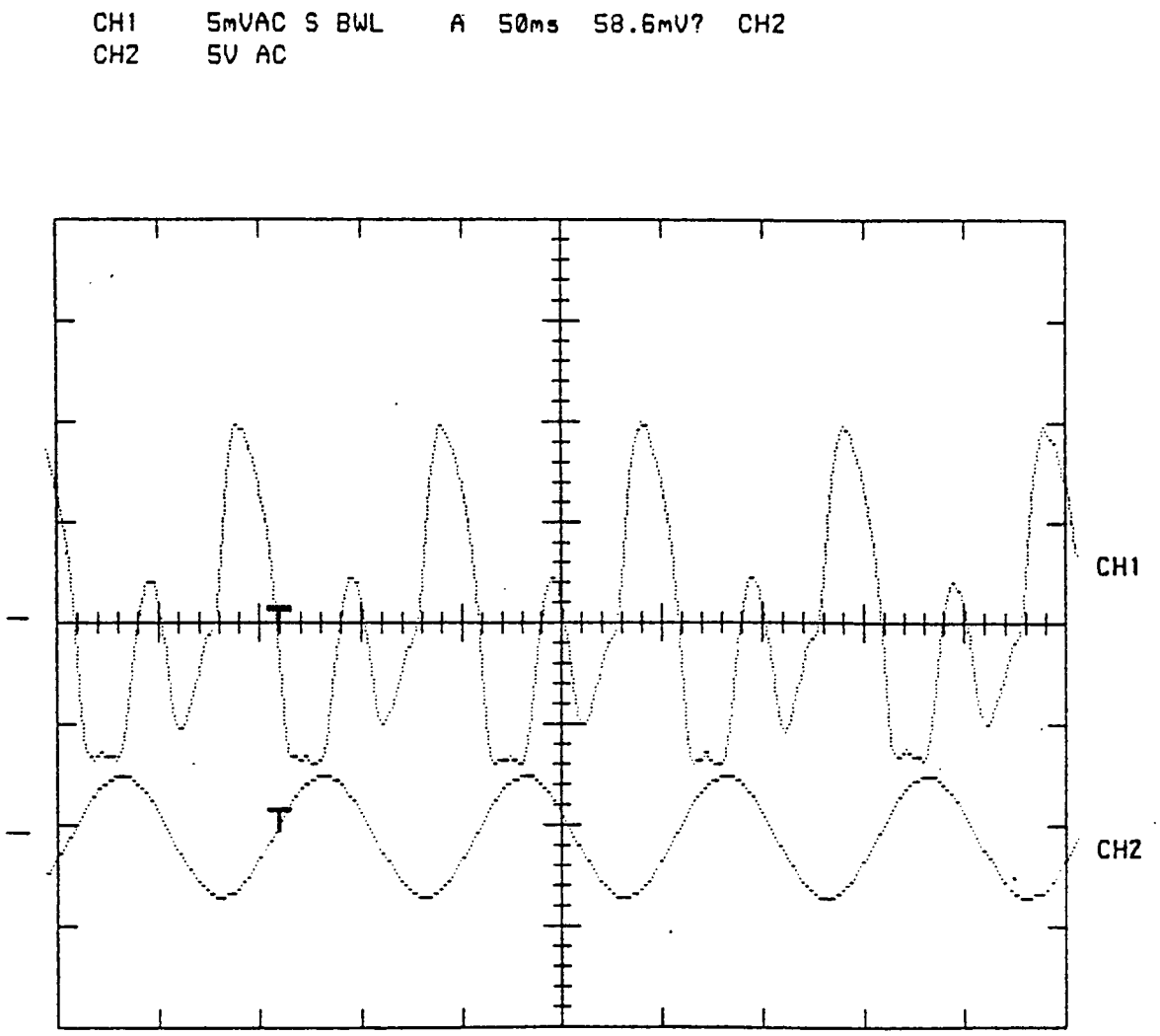

Fig. 5.16 Waveform distortion observed with a dc bias of 225.6 Oe and a higher ac field

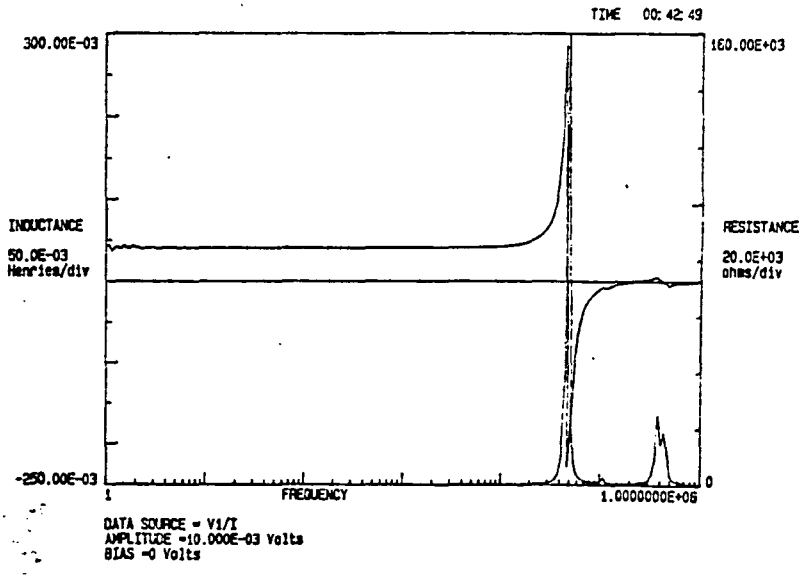

Fig. 5.17 Inductance and resistance of solenoid with nothing inside

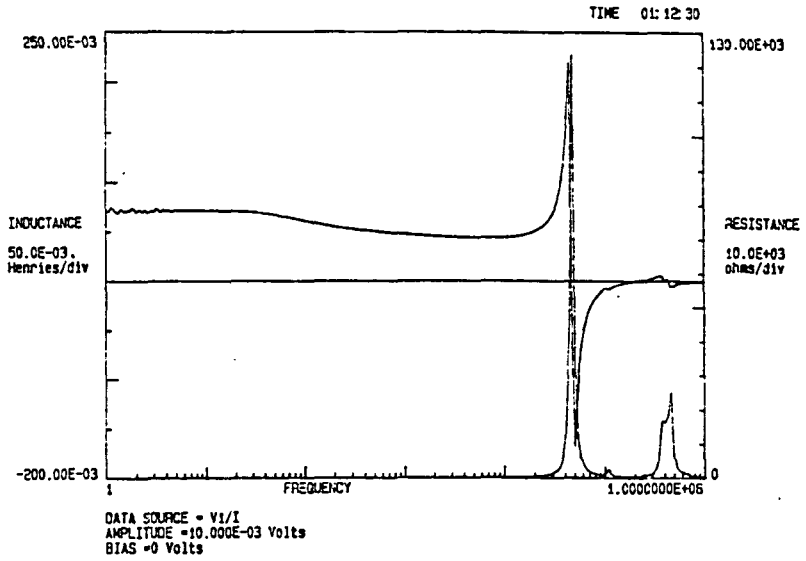

Fig. 5.18 Inductance and resistance of solenoid with 1 steel rod inside

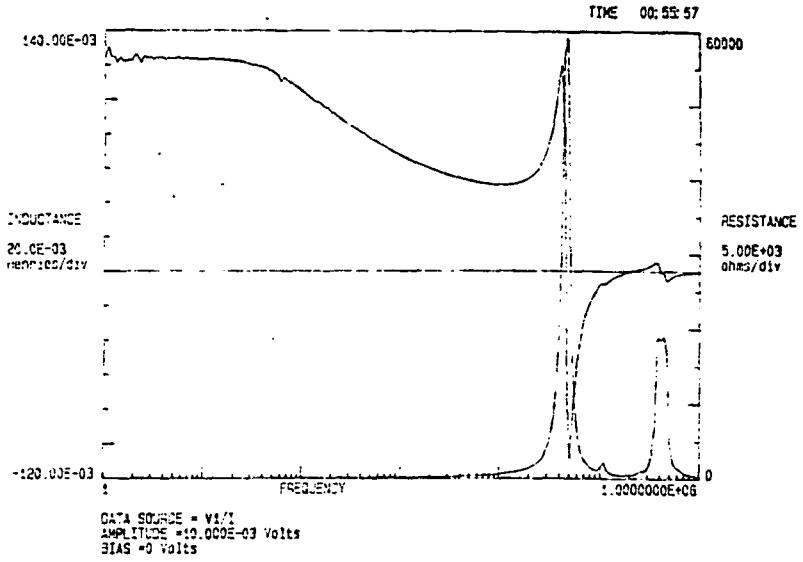

Fig. 5.19 Inductance and resistance of solenoid with 4 steel rods inside

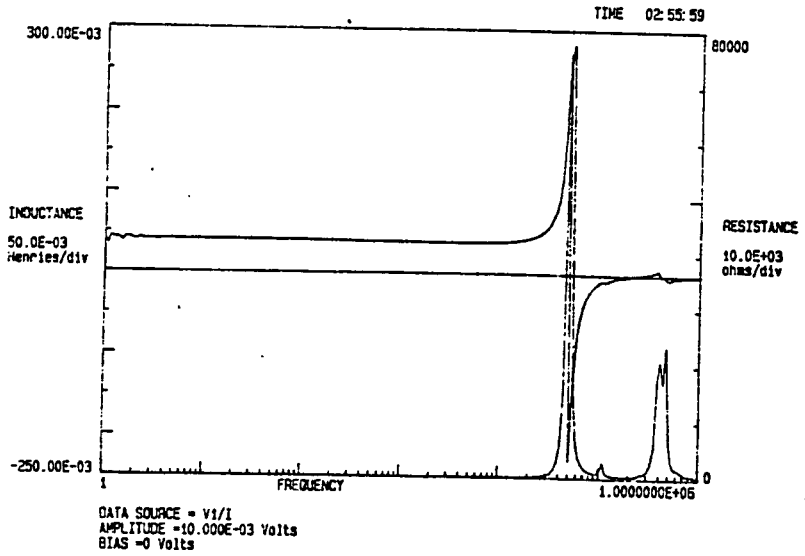

Fig. 5.20 Inductance and resistance of solenoid with Hall probe inside

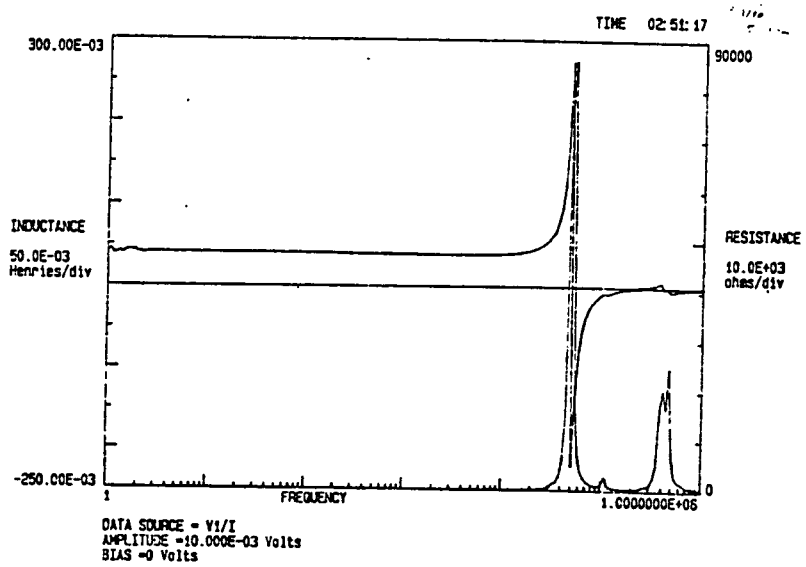

Fig. 5.21 Inductance and resistance of solenoid with magnetometer inside

results are shown in Fig. 5.17 - Fig. 5.21. The solenoid was tested with these conditions: a.) nothing in the core, b.) 1 steel rod in the core, c.) 4 steel rods in the core, d.) a Hall probe in the core, and e.) the magnetometer in the core. It was observed that the magnetometer did not alter the characteristics (i.e., inductance and capacitance) of the solenoid.

5.7 Experimental Study on the Diode Laser Sensor

As mentioned in the previous context, both the Terfenol-D performance and the diode sensor performance were critical to the overall functioning of the magnetometer. However, the evaluation of the diode sensor is very difficult since one has to reproduce the movement of the external reflector with a resolution of about 0.1 micrometer. This was accomplished with the experimental setup as shown in Fig. 5.22. A gold-plated plane mirror mounted on a x-y-z positioner with 1 micrometer resolution was used to simulate the external reflector. The distance between the laser facet and the mirror was adjusted so that the mirror was almost touching the laser facet, and the out-of-phase condition was obtained. It is recommended that this experiment be carried out on a floating optical table since the vibration from closing the door or a human voice can vibrate the mirror and produce significant noise. Once the out-of-phase condition was found, the mirror was moved away from the laser facet by turning the knob of the x-y-z positioner while the pattern was stored on a sampling scope. The experiment results are displayed in Fig. 5.23 and Fig. 5.24. The in-phase and out-of-phase condition were shown very clearly. However, the result was contrary to reference [11], which failed to predict the exponential decay of the output signal as the external cavity lengthens. Also, as the external cavity got longer, the in-phase and out-of-phase condition was hard to distinguish. However, the average of the output signal was larger than the output

signal without external cavity. This point was already mentioned in the previous context. The experimental result reported here is very similar to that published by Voumard, Salathe and Weber **[13]**. However, to the best of the experimenters' knowledge, no such detailed experimental result has been published. The result of this measurement is very significant because it raises the question of validity in the modelling of this device as reported in **[11]**. Also, it provides very valuable information on the operational characteristics of the magnetometer. The physics of the magnetometer's operation became more complicated due to the nonlinear interaction of the cavity length and output power. The situation can become quite complicated since the dc bias for the Terfenol-D rod alters the dc length of the rod, which, in turn, alters the external cavity length. As a result, one has to take extreme care in interpreting the preliminary results of the magnetometer prototype evaluation. To properly understand the operation of this device and to interpret the data properly, one has to model the diode sensor numerically, which is covered in the next chapter.

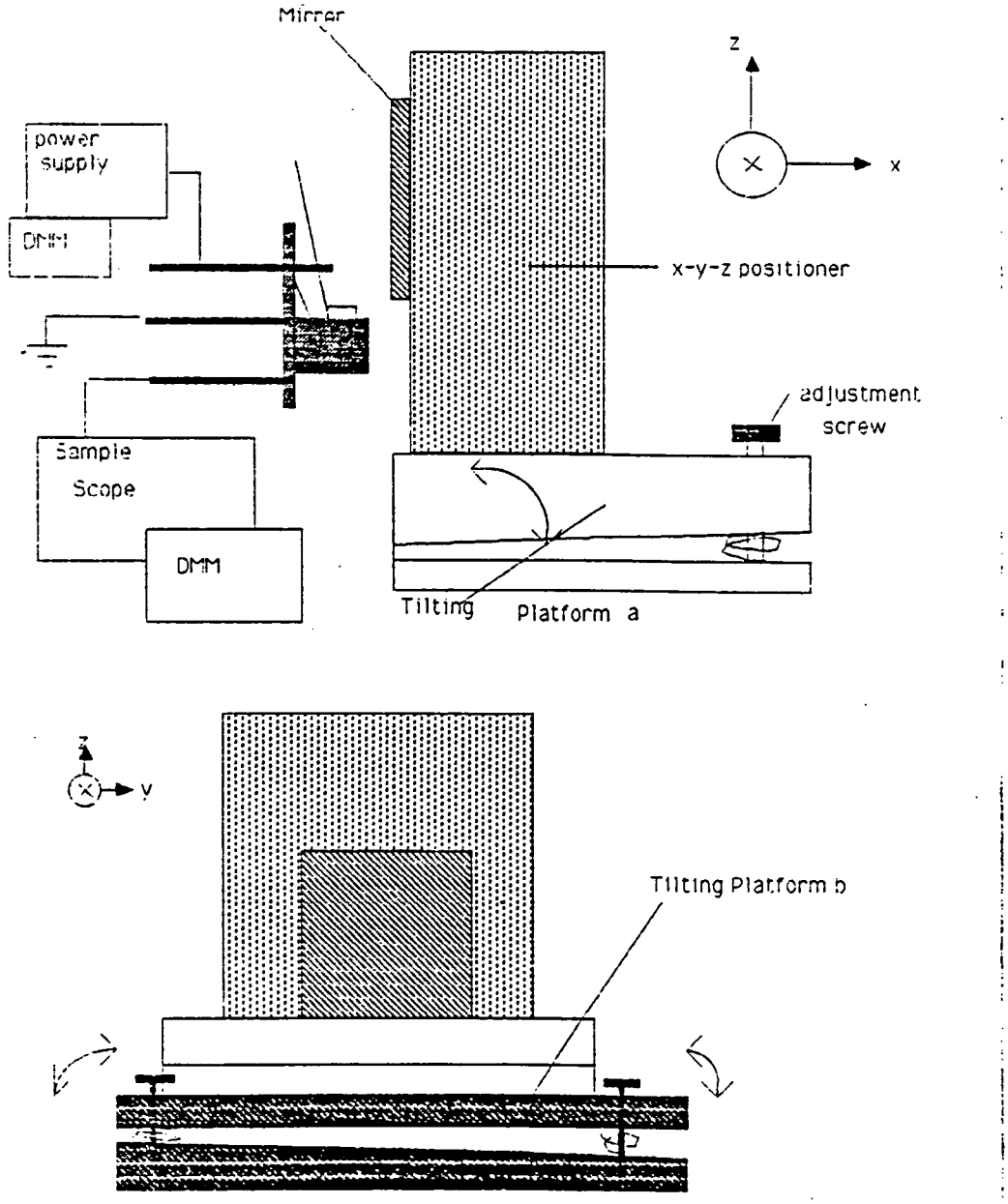

Fig. 5.22 Experimental setup used to study the external cavity laser

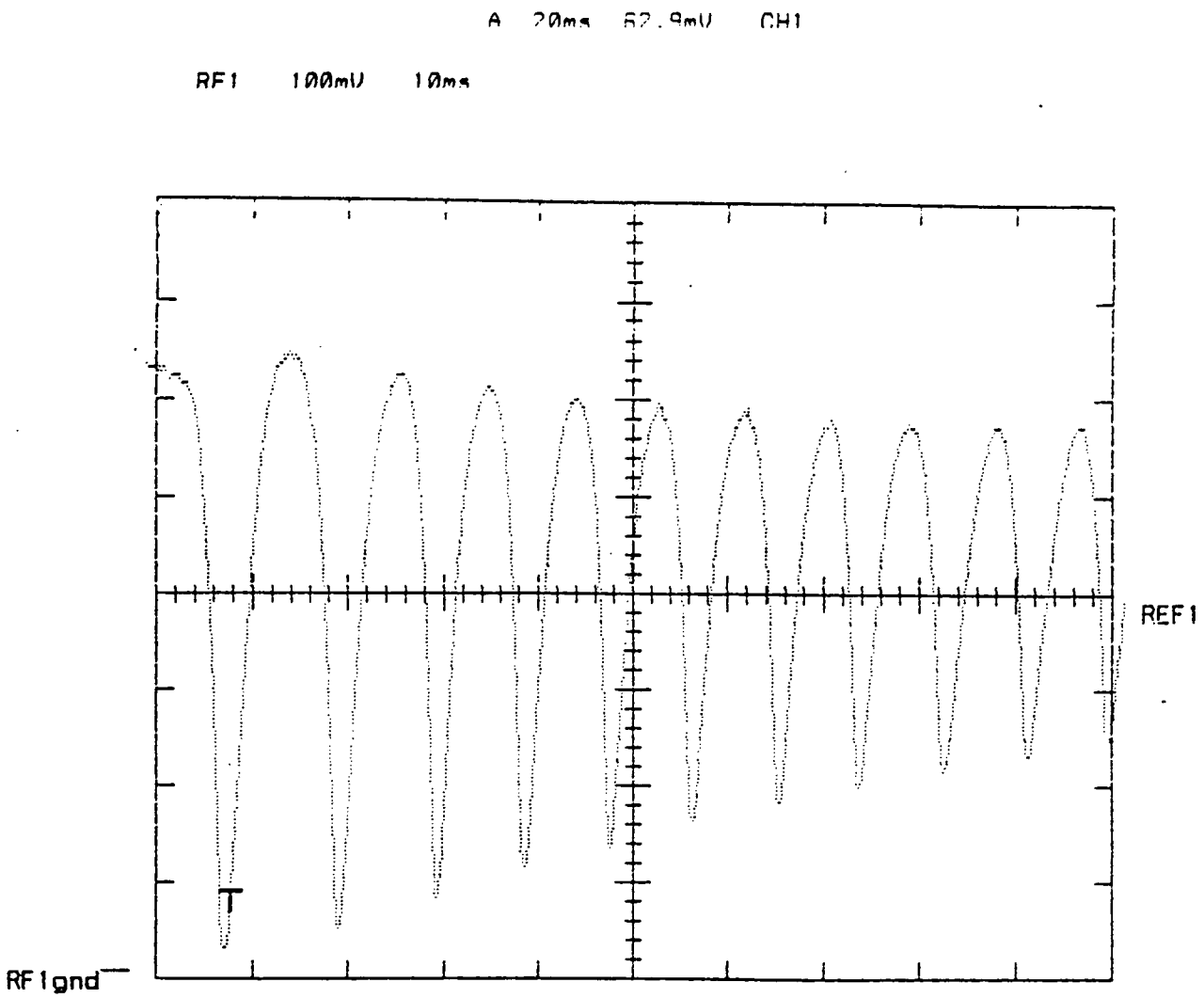

Fig. 5.23 Plot of photodetector voltage of the external cavity laser sensor (with short cavity)

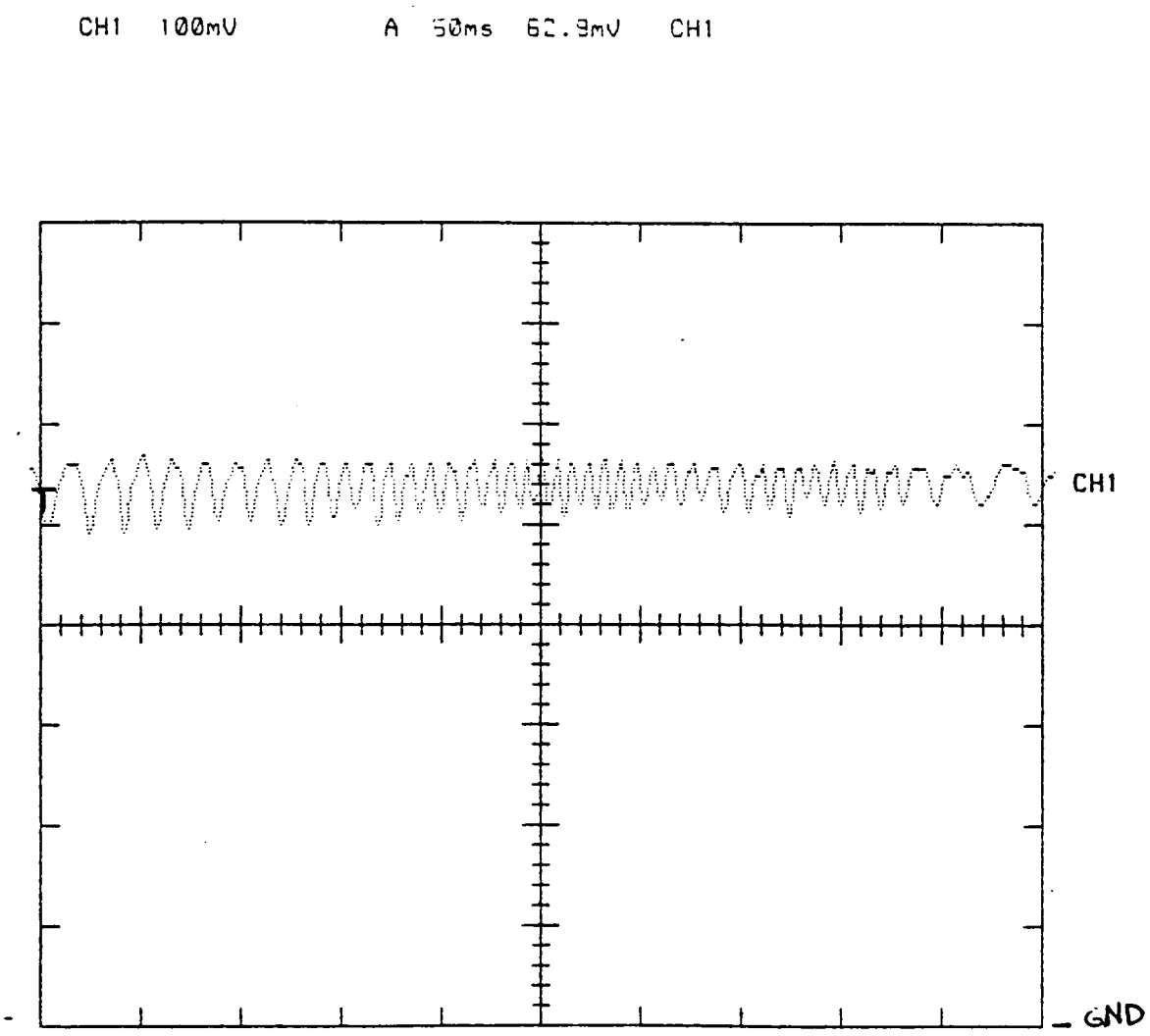

Fig. 5.24 Plot of photodetector voltage of the external cavity laser sensor (with long cavity)

6. INTRODUCTION TO THE MODELLING OF LASER DIODE MAGNETOMETER TERFENOL-D MAGNETOMETER

As mentioned in the above, the physics of this simple device is not so straightforward. Many experiments have been done to evaluate the performance of the magnetometer, and many phenomena are reported in the above chapters. The purpose of this chapter is to discuss the aspect of modelling the performance of the magnetometer. The problem can be separated into two areas: 1.) modelling of the Terfenol-D rod movement. 2.) modelling of the laser diode sensor operation. The modelling of the Terfenol-D rod movement is not covered here. This portion of modelling is carried out by specialists in this area [14]. The rest of this thesis focuses on the modelling aspect of the laser diode sensor only.

6.1 A Proper Model

To model the laser diode sensor, one has to understand thoroughly the underlying physics of the laser diode. Using a very primitive and approximate approach, one can understand the operation of the sensor as follows: when the effective facet reflectivity is high, more light energy is being trapped inside the laser cavity. As a result, the output power at the other end of the mirror, which has maintained the same reflectivity, is increased. When the reflectivity is low, most of the light energy leaks out of the cavity, the amount of light reflecting back to the cavity is low and stimulated emission is reduced. Therefore, the laser diode is operating as a superluminescent LED. This explanation can help in understanding the basic principle of the laser diode sensor operation. However, it already raises a lot of questions in the modelling of the sensor. For example, in reference 11 [11], the diode

sensors were modelled using the conventional laser rate equation and with the assumption that spontaneous emission was very small, and can therefore be neglected. However, when the effective reflectivity of the diode laser facet is reduced, stimulated emission is lowered. Consequently, the spontaneous emission constitutes a major part of the emission power. Ignoring the effect of the spontaneous emission may not be very correct. Furthermore, as the effective reflectivity is increased, the internal light intensity of the cavity increases and this implies the photon density is increased.

A further question arises about taking into account gain saturation. Again, a simple rate equation approach cannot answer this question. Moreover, the rate equation totally neglects the spatial variation of photon density and gain distribution along the cavity length. If the mirror reflectivity of the laser diode is high, the regular rate equation can be used without much problem. However, as the mirror reflectivity is changed from a high value to a low value, a simple model which ignores spatial variation may not be adequate (see Fig. 6.1) [15]. The validity of the simple rate equations has been discussed by many authors, such as Marcuse [16], Cassidy [17], and Sommers [18]. In the formulation by Marcuse [16], he suggested modelling the laser amplifier or oscillator with a time and space traveling wave equation which used the time dependent rate equation at a particular point in the laser cavity, and then applying a traveling wave equation to sum up the effects of all points. Also, Marcuse considers a multimode laser instead of a single mode laser. This is a very complete model since it takes into account almost everything besides gain saturation which can be incorporated into the modelling process without much difficulty [19]. The incorporation of the mutlimode effect is an important point because it has been demonstrated that the mirror reflectivity affects the width of the line-shape function [20] and it was reported that if the facet reflectivity of a laser diode was substantially reduced, then the laser exhibited multimode operation [21]. However, the formulation of Marcuse's model leads to a set of non-linear coupled equations,

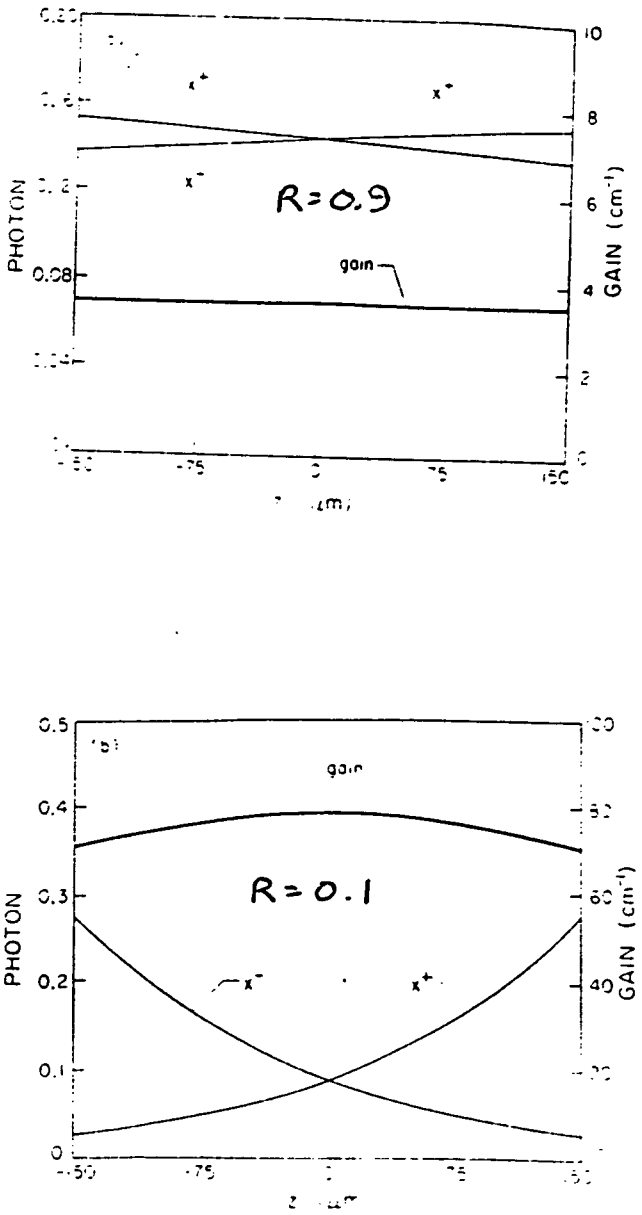

Fig. 6.1 Static photon and electron density distribution inside the laser diode

which cannot be solved easily even with numerical methods. Therefore, it is very hard to obtain the physics from Marcuse's formulation to explain some of the observed phenomenon.

Cassidy has suggested the application of Fabry-Perot approaches to modeling a diode laser rather than the rate equation approach [5]. He has shown that the time dependent rate equation ignores the effect of ASE. Also, Cassidy [17] has developed an analytical solution to the modeling of the laser diode which avoids the non-linear coupled equations and numerical convergence problem in Marcuse's model. He suggested the main perturbation in a laser diode with mirror reflectivity changes, was the effective spontaneous emission, which is the spontaneous emission power coupled to one of the guided modes of the cavity. He explained that as the reflectivity was increased, the threshold for lasing was decreased and maintaining the same pumping level produced higher inverted population. As the population at the upper level increases, the chance for spontaneous emission increases. With higher spontaneous emission power, the effective spontaneous power received by each guided mode increases. Therefore, the laser will tend to run multimode [22]. This probably explains the reason for not observing the out-of-phase condition in the evaluation of the laser diode with external cavity (about 50 micrometer long) since the power contributed from the side modes increases but the out-of-phase condition only affects a single frequency (i.e., the fundamental mode).

The actual implementation and the result of the modeling are not discussed here. It should be noted that to model the laser diode means studying the output spectrum, the light output power and the spatial distribution of the photon density and electron density in the longitudinal direction. The studying of the beam spot size, near-field pattern and far-field pattern requires the knowledge of the waveguiding mechanism and the injected current diffusion in the transverse and lateral directions.

7. FUTURE WORK

This prototype has demonstrated the feasibility of applying Terfenol-D and a low-cost laser diode in fabricating a magnetometer. However, this is not the ultimate goal of this project. Future work includes the fabrication of a three dimensional portable magnetometer based on the technology described here. Also, the physics of the magnetometer should be explored further. In addition, means for improving magnetometer sensitivity or a second generation prototype should be explored. Moreover, calibration equipment should be developed for calibrating the magnetometer. Modelling of both the magnetostrictive response of the Terfenol-D sensor and of the laser cavity are desirable.

8. CONCLUSIONS

In this research work, the feasibility of a miniature optical magnetostrictive magnetometer, using Terfenol-D as the magnetostrictive element and a diode laser as a sensor, was explored. A magnetometer prototype utilizing the above elements was fabricated and evaluated. The prototype has demonstrated the feasibility of detecting magnetic field intensity in ten milli-Oersted range, which corresponds to a transducer movement of approximately 0.1 Angstrom. These figures are deduced from the evaluation result of the Terfenol-D rod under 1 Oe magnetic field intensity using a heterodyne interferometer.

In addition, an experimental study on the performance of the diode laser sensor was carried out and a non-linear output of the sensor was observed. These experimental results are reported for the first time. The experimental result obtained from the evaluation process indicated that a precise model of the external cavity laser diode sensors is needed.

9. BIBLIOGRAPHY

1. Verdeyen, J. T. Laser Electronics. Englewood Cliffs, New Jersey: Prentice Hall, 1989

2. Eisberg, R. M. Fundamentals of modern physics New York: John Wiley & Sons, 1961

3. Breene, R. G. , Jr. "Line Shape." Review of Modern Physics 29, 94-143, 1957.

4. Siegman, A. E. Lasers. Mill Valley, California: University Science Books, 1986

5. Cassidy, D. T. "Comparison of rate-equation and Fabry-Perot approaches to modelling a diode laser." Applied Optics 22, No. 21, 3321-3326, 1983

6. Sze, S. M. Physics of Semiconductor Devices. New York: John Wiley & Sons, 1982

7. Dagenais, D. M., F. Bucholtz and K. P. Koo "Heterodyne Detection of Magnetic Fields from 0.1 Hz to 10 MHz in a Magnetostrictive Fiber Sensor." To be published in IEEE Journal of Lightwave Technology

8. Jiles, D. C. private communication: Dr. Jiles had measured the saturation magnetostriction of nickel and Terfenol-D, and estimated the ratio.

9. Verhoeven, J. private communication: These data were given to the author during a meeting on patenting the magnetometer

10. Koo, K. P., F. Bucholtz , A. Dandridge and A. B. Tveten "Stability of a Fiber-Optic Magnetometer" IEEE Transactions on Magnetics, MAG-22, No. 3 , 141-144, 1 986

11. Miles, R. O., A. Dandridge, A. Tveten and T. Giallorenzi "An External cavity Diode Laser Sensor" IEEE Journal of Lightwave Technology, LT-1, No. 1, 81-92, 1983

12. Jiles, D. C. private communication: Dr. Jiles calculated the approximate value for the dc optimum biasing

13. Voumard, C., R. Salathe, and H. Weber "Resonance Amplifier Model Describing Diode Lasers Coupled to Short External Resonator." Applied Physics, 12, 369-378, 1977

14. Jiles, D. C. private communication: Dr. Jiles have shown the author some unpublished results on computer modelling of ac magnetostrictive behavior

15. Lau, K. Y. and A. Yariv "High-Frequency Current Modulation of Semiconductor Injection Lasers." in Semiconductors and Semimetals, vol 22. Pt. B, chapter 2.

16. Marcuse, D. "Computer Model of an Injection Laser Amplifier." IEEE Journal of Quantum Electronics, QE-19, No. 1, 63-73, 1983

17. Cassidy, D. T. "Analytic Description of a Homogeneously Injection Laser." IEEE Journal of Quantum Electronics, QE-20, No. 8, 913-918, 1984

18. Sommers, H. S. "Threshold and Oscillation of Injection Lasers: A Critical Review of Laser Theory." Solid State Electronics, Vol. 25, No. 1, 25-44, 1982

19. Chung, R. unpublished: The author followed the method outlined by Marcuse and implemented a computer program to model the laser oscillator with saturation effect taken in account

20. Petermann, K. Laser Diode Modulation and Noise. Tokyo: KTK Scientific Publisher, 1989

21. Ettenberg, M. E. "The Effect of Facet Mirror Reflectivity on the Spectrum of Single-Mode CW Constricted Double-Heterojunction Diode Lasers." IEEE Journal of Quantum Electronics, QE-17, No. 11, 2211-2214, 1981

22. Cassidy, D. T. "Explanation of the Influence on the Oscillation Spectrum of Facet Reflectivity." Journal of Applied Physics, 57, No. 3, 1985

10. ACKNOWLEDGEMENTS

I would like to express my appreciation to both of my major professors Dr. John Lamont and Dr. Robert Weber for their financial support and technical guidance in this research work. I also want to thank Dr. Stanley Burns for providing me a teaching assistantship during last summer. I am also very grateful to Dr. Stanley Burns, Dr. D. C. Jiles, Dr. J. Shinar and Dr. J. Verhoeven for serving on my committee.

I would like to thank Dr. D. C. Jiles and Ames Laboratory for providing laboratory space and measuring equipments during the course of this research work. Also, I would like to thank Dr. Verhoeven for providing the Terfenol sample. Moreover, I would like to express my sincere gratitude to Mike in Ames Laboratory Student Machine Shop for fabricating such a high quality magnetometer housing for this research.

Many of the optical measurements and experiments were carried out in the Optics and Thermal Wave Laboratory in the NDE center. I would like to thank Mr. John Moulder and Dr. Mike Hughes of NDE center for allowing me to use their equipment and laboratory space, Mr. Mark Kobuvich for his assistance in taking pictures of the de-capsulated laser diode, and Mr. Jin-Yong Kim for his participation in the evaluation process of the prototype and in the experimental study of the laser diode sensor. It should be mentioned that the idea of using the sampling scope to obtain the output signal was originated by Mr. Kim.

I would like to thank Dr. W. Lord, Dr. D. C. Jiles, Dr. J. Verhoeven, Dr. Hsu of NDE center, Dr. B. Thompson of Ames Lab., Mr. John Moulder, Suresh and Jennifer of Dr. Jiles' Lab for their helpful advice during the course of this project.

Last but not least, I would like to thank my family for their moral support, my fiance for her understanding and encouragement, and my teacher Tdu Fuk Lua for his teaching and guidance.

11. APPENDIX

TECHNICAL SPECIFICATION OF LASER DIODE ML-4402 FROM MITSUBISHI

ML-4402

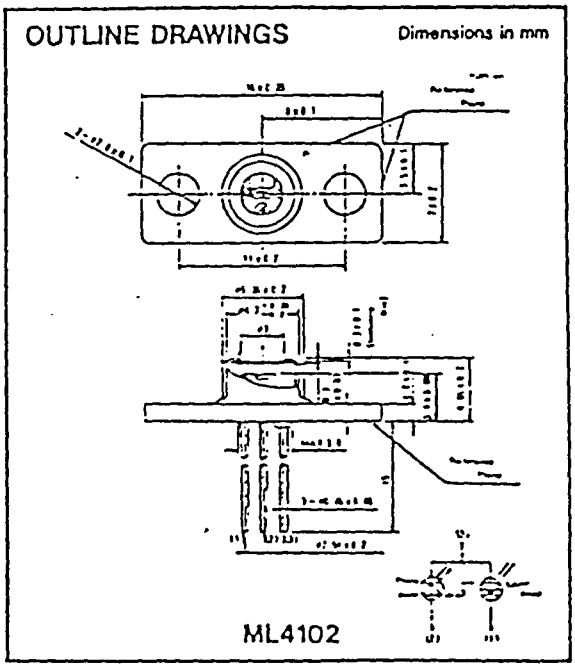

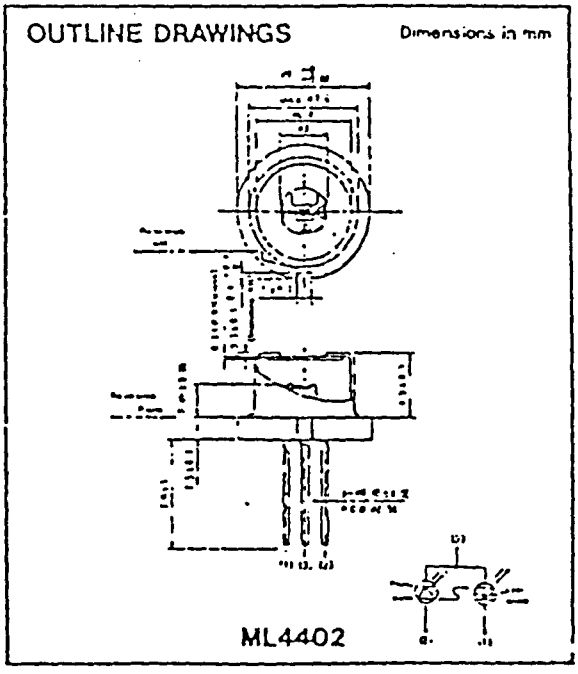

ML-4402

OUTLINE DRAWINGS Dimensions in mm

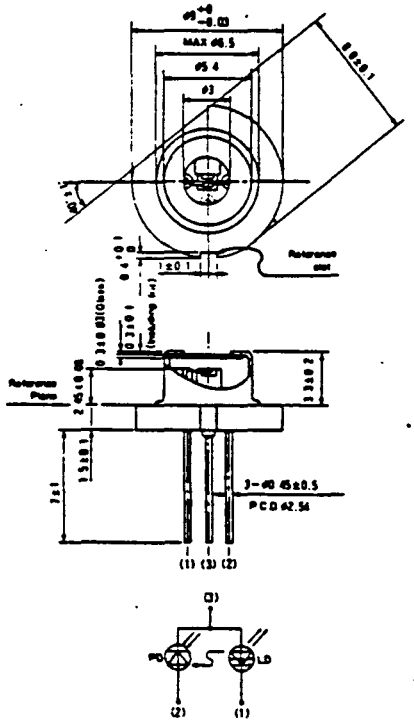

ML4422

OUTLINE DRAWINGS Dimensions in mm

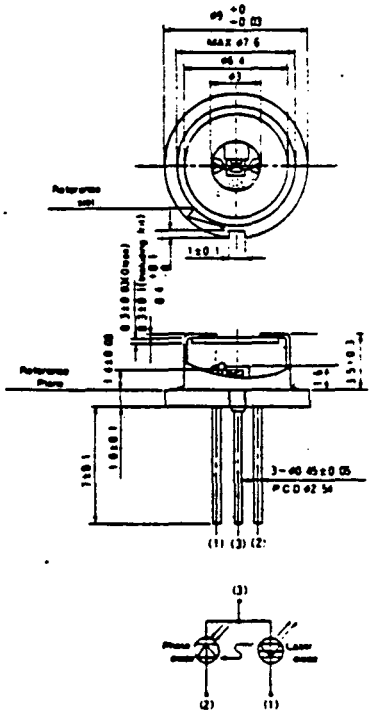

ML4432

ML-4402

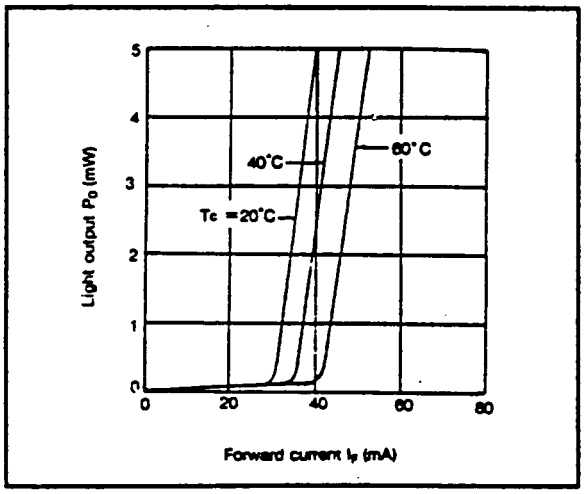

Fig. 1 Light output vs forward current

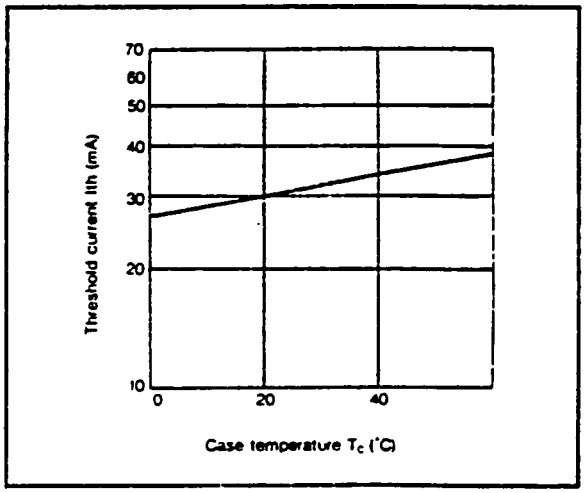

Fig. 2 Temperature dependence of threshold current

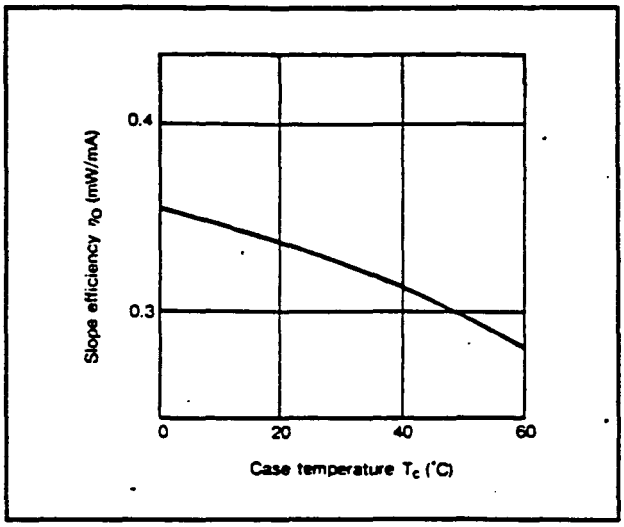

Fig. 3 Temperature dependence of slope efficiency

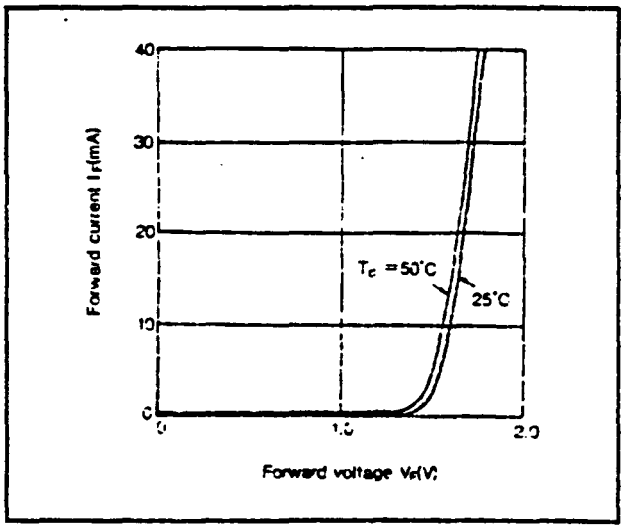

Fig. 4 Forward current vs voltage characteristics

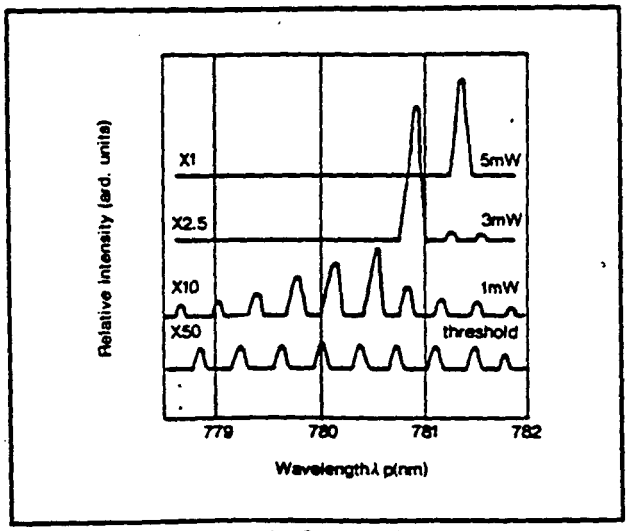

Fig. 5 Emission spectra under CW operation

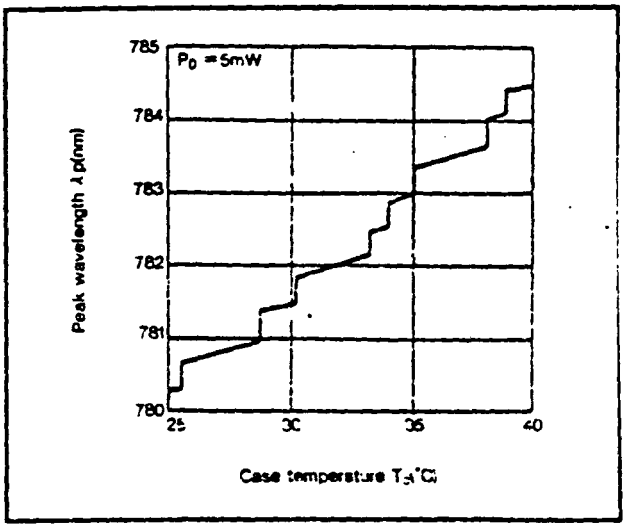

Fig. 6 Temperature dependence of peak wavelength

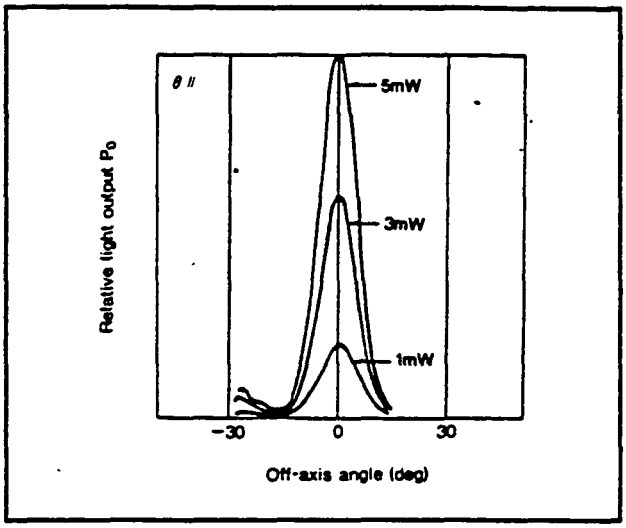

Fig. 7 Far-field patterns in plane parallel to heterojunctions

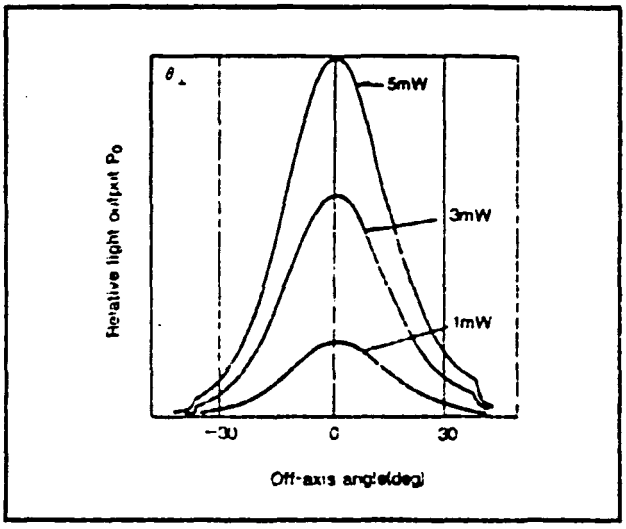

Fig. 8 Far-field patterns in plane perpendicular to heterojunctions

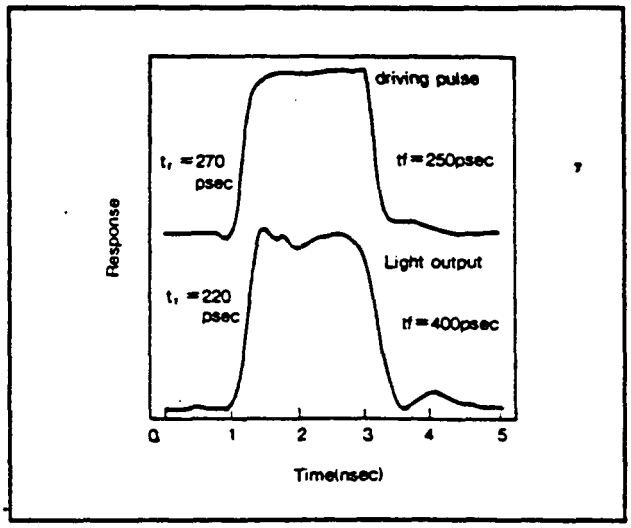

Fig. 9 Pluse response waveform

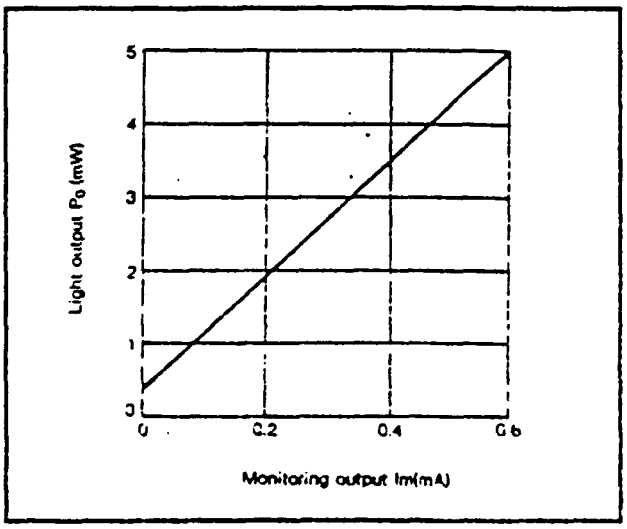

Fig. 10 Light output vs. monitoring output current

ML-4402

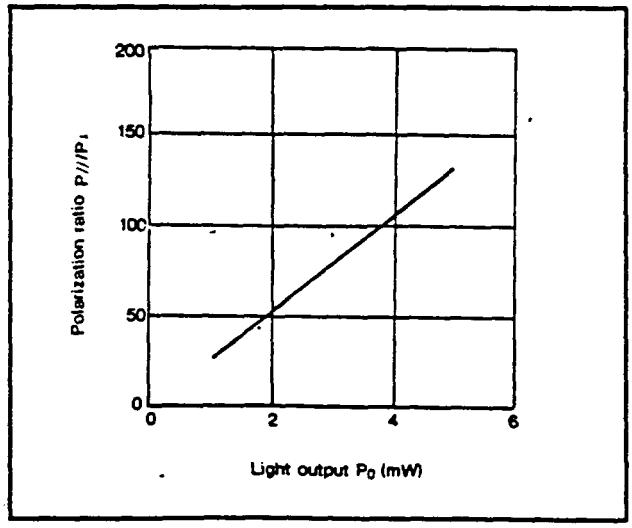

Fig. 11 Polarization ratio vs. light output

ELECTRICAL/OPTICAL CHARACTERICS (T_c=25°C)

Symbol	Parameter	Test conditions	Limits			Unit
			Min.	Typ.	Max.	
I_{th}	Threshold current	CW	–	30	60	mA
I_{op}	Operating current	CW, P_O=3mW	–	40	70	mA
V_{op}	Operating voltage (Laser diode)	CW, P_O=3mW	–	1.8	2.5	V
I_D	Dark current (Photo diode)	V_{RD}=10V	–	–	0.5	μA
P_O	Light output	CW, I_F=I_{th}+10mA	–	3	–	mW
λ_p	Lasing wavelength	CW P_O=3mW	765	780	795	nm
$\theta_{//}$	Full angle at half maximum	CW P_O=3mW	8	11	15	deg
$\theta_{\perp}$			20	33	45	deg
C_t	Capacitance (Photo diode)	V_R=0V, f=1MHz	–	7	–	pF
I_m	Monitoring output current	CW, P_O=3mW V_{RD}=1V, R_L=10Ω (Note2)	0.15	0.35	0.7	mA

Note2 : R_L is load resistance of the photodiode.